Copyright Warning & Restrictions

The copyright law of the United States (Title 17, United States Code) governs the making of photocopies or other reproductions of copyrighted material.

Under certain conditions specified in the law, libraries and archives are authorized to furnish a photocopy or other reproduction. One of these specified conditions is that the photocopy or reproduction is not to be "used for any purpose other than private study, scholarship, or research." If a, user makes a request for, or later uses, a photocopy or reproduction for purposes in excess of "fair use" that user may be liable for copyright infringement,

This institution reserves the right to refuse to accept a copying order if, in its judgment, fulfillment of the order would involve violation of copyright law.

Please Note: The author retains the copyright while the New Jersey Institute of Technology reserves the right to distribute this thesis or dissertation

Printing note: If you do not wish to print this page, then select "Pages from: first page # to: last page #" on the print dialog screen

NJIT New Jersey's Science & Technology University

The Van Houten library has removed some of the personal information and all signatures from the approval page and biographical sketches of theses and dissertations in order to protect the identity of NJIT graduates and faculty.

ABSTRACT

Radiation from
A Tapered Dielectric Rod Antenna

by
Anil Prabhakar

The radiation fields from a cylindrical dielectric taper is studied. The numerical results of a theoretical model for a taper excited by the dominant HE_{11} mode is compared with experimental measurements. A theoretical model for the next propagating mode in the structure, the TE_{01} mode, is investigated and numerical results based on this proposed model are generated. The theoretical models are based upon the combination of the exact modal field solutions for a step profile cylindrical dielectric rod waveguide, *local mode theory*, and the *equivalence principle* for the determination of equivalent current densities.

The far-zone radiation field is considered to be the summation of the two radiative components in the dielectric rod/cone structure. The "aperture" of the uniform dielectric rod at the transition plane (rod/cone interface) and the dielectric taper itself. In the former case, the field is obtained from the equivalent surface current densities on the aperture surface, whereas in the latter case, the field is obtained from the equivalent volume polarization current density induced in the conical structure.

Numerical results are obtained using a number of different input data sets, where the parameters such as the free-space wavelength λ, the refractive index of the dielectric n_1 and the length of the taper are varied. These are then compared against the experimental observations and a satisfactory agreement between the two sets of data is achieved.

RADIATION FROM A TAPERED DIELECTRIC ROD ANTENNA

by
Anil Prabhakar

A Thesis
Submitted to the Faculty of
New Jersey Institute of Technology
in Partial Fulfillment of the Requirements for the Degree of
Master of Science in Electrical Engineering

Department of Electrical and Computer Engineering

October 1993

APPROVAL PAGE

Radiation from
A Tapered Dielectric Rod Antenna

Anil Prabhakar

Dr. Edip Kiver, Thesis Advisor (date)
Associate Professor of Electrical Engineering, NJIT

Dr. Gerald Whitman, Committee Member (date)
Professor of Electrical Engineering, NJIT

Dr. Gary Wu, Committee Member (date)
Assistant Professor of Electrical Engineering, NJIT

BIOGRAPHICAL SKETCH

Author: Anil Prabhakar

Degree: Master of Science in Electrical Engineering

Date: October 1993

Date of Birth:

Place of Birth:

Undergraduate and Graduate Education:

- Master of Science in Electrical Engineering,
  New Jersey Institute of Technology, Newark, NJ, 1993
- Bachelor of Technology in Engineering Physics,
  Indian Institute of Technology, Bombay, India, 1992

Major: Electrical Engineering

ACKNOWLEDGMENT

I wish to express my sincere gratitude to my advisor Dr. Edip Niver, for his helpful suggestions, his guidance and his patience during the course of this thesis. I take the opportunity to thank my friends and the members of my family for their constant support and encouragement. Financial assistance from the New Jersey Institute of Technology, Newark is also gratefully acknowledged.

TABLE OF CONTENTS

Chapter		Page
1	INTRODUCTION	1
2	FORMULATION OF THE PROBLEM	3
3	THE CYLINDRICAL DIELECTRIC WAVEGUIDE	7
	3.1 Modal Field Solutions of the Cylindrical Waveguide	7
	3.2 General Eigenvalue Equations	11
	3.3 HE_{11} Modal Fields and Eigenvalues	13
	3.4 TE_{01} Modal Fields and Eigenvalues	15
	3.5 Modal Power Flow	15
	3.5.1 HE_{11} mode	16
	3.5.2 TE_{01} mode	17
4	THE DIELECTRIC TAPER	18
	4.1 Local Mode Field Solutions	18
	4.2 Power Conservation	20
5	FAR FIELD RADIATION	22
	5.1 Far Field Radiation due to the Surface Currents $\mathbf{J}_s'.\mathbf{M}_s'$	23
	5.1.1 HE_{11} mode	24
	5.1.2 TE_{01} mode	24
	5.2 Far Field Radiation due to the Volume Current Density $\mathbf{J}_v$	25
	5.2.1 HE_{11} mode	25
	5.2.2 TE_{01} mode	26
	5.3 Directive Gain	27
6	NUMERICAL AND EXPERIMENTAL RESULTS	28
	6.1 Radiation Pattern of a Circular Guide	28
	6.2 HE_{11} Mode Radiation Pattern	29

Chapter Page

6.3 Radiation from the Tapered Dielectric 33

6.4 TE_{01} Mode Radiation Pattern 42

7 CONCLUSIONS 47

REFERENCES 49

LIST OF FIGURES

Figure		Page
2.1	Tapered uniform cylindrical dielectric rod/cone geometry.	4
2.2	Decomposition of the dielectric rod/cone structure: (a) The dielectric rod in the $z < 0$ region. (b) The tapered dielectric in the $z > 0$ region.	5
2.3	The dielectric cone: (a) Actual problem. (b) Volume equivalence model.	6
3.1	(a) Infinitely long uniform cylindrical rod waveguide (b) Refractive index profile.	8
4.1	The approximate model for the dielectric cone.	19
6.1	Experimental antenna assembly	28
6.2	TE_{11} mode far field radiation pattern	30
6.3	Radiation pattern of the mode converter	32
6.4	Experimental set-up	35
6.5	HE_{11} mode radiation pattern for plexiglass. l=2.8cm	36
6.6	HE_{11} mode radiation pattern for plexiglass. l=1.9cm	37
6.7	HE_{11} mode radiation pattern for plexiglass. l=1.5cm	38
6.8	HE_{11} mode radiation pattern for teflon. l=2.8cm	39
6.9	HE_{11} mode radiation pattern for teflon. l=1.9cm	40
6.10	HE_{11} mode radiation pattern for teflon. l=1.5cm	41
6.11	TE_{01} mode radiation pattern, l=2.8cm	44
6.12	TE_{01} mode radiation pattern, l=1.9cm	45
6.13	TE_{01} mode radiation pattern, l=1.5cm	46

CHAPTER 1

INTRODUCTION

The dielectric rod antenna consists of a dielectric cylinder excited by a microwave guide, usually a hollow waveguide. The radiation characteristics of such an antenna have been studied extensively over a long period. It was observed that by shaping the radiating end of the dielectric rod, the radiation characteristics improved considerably giving better directivity and beam-width. However, these studies were conducted on a dielectric rod excited with the TE_{11} mode from a hollow waveguide [1]. The fundamental propagating mode in a cylindrical dielectric structure is the HE_{11} mode which has no cut-off frequency. The next propagating mode is the TE_{01} mode [2]. Efforts have also been made to study the radiation pattern due to these modes.

Yaghjian and Kornhauser [3] studied the problem of a circular semi-infinite dielectric rod antenna excited by the hybrid HE_{11} mode from a hollow waveguide. Based on the postulation that the tapering of the radiating end would match the impedance of the dielectric rod to that of free space, Georghiades [4] and Hoydal [5] predicted the radiation patterns of the dielectric tapered rod antenna excited by the HE_{11} mode. They made use of the *local mode theory* in conjunction with equivalent surface and volume current distributions. Previous studies indicate that the *local mode theory* is quite useful in applications involving tapered geometries.

The results of the methods used in [4] and [5] are compared here with the experimentally measured radiation patterns of the tapered dielectric rod antenna. The *local mode theory* has also been used to extend this formulation to the next propagating mode and thereby predict the radiation patterns for dielectric antennas excited by the TE_{01} mode. The observation of a main lobe along the axis of the dielectric cone, in the case of the HE_{11} mode, supports the assumptions made of

an adiabatic tapering of the dielectric. The conical structure is approximated by a series of thin concentric cylinders. The radiation field is then synthesized as the superimposition of the fields from the dielectric-rod and from the conical taper. The tapering must be sufficiently slow so as to avoid higher-order coupling effects.

The model for the excitation by the TE_{01} mode predicts the existence of multiple lobe formations. While the lobes near the axis of the cone are well defined, those that are oriented at an angle to the axis are thin and somewhat random in shape. The angular distribution of the far-field radiation pattern is dependent on various parameters like the length of the taper, frequency of operation and the refractive index of the material. Further studies are necessary to understand the higher order mode radiation in tapered environments due to the complex transitions involving propagating and evanescent fields.

CHAPTER 2

FORMULATION OF THE PROBLEM

Consider the combined dielectric rod/cone geometry depicted in Fig.2.1. It consists of a uniform dielectric rod with core radius a and refractive index n_1 immersed in an infinite medium of refractive index n_2. At $z = 0$ the dielectric rod begins to taper linearly into a cone. In order to consider only the guided modes in the rod, the condition $n_1 > n_2$ must be satisfied. In general, the waveguide can support multiple modes depending on the media parameters n_1, n_2, the free-space wavelength λ and the rod radius a. The HE_{11} mode is called the fundamental mode of a cylindrical dielectric waveguide because it is the only mode without a cutoff condition. The next propagating mode is the TE_{01} mode that has a cutoff for a wavelength defined by parameters such as the radius of the rod and the refractive indices of the rod and the medium surrouding it.

Let $\mathbf{E_i}, \mathbf{H_i}$ represent the incident vector fields of a possible mode propagating in the $+z$ direction. As this incident surface wave propagates into the tapered region, a fraction of the field is reflected back in the $-z$ direction while the rest is considered to be transmitted further and will be referred to as scattered fields in the text. The scattered fields are represented by $\mathbf{E_s^-}, \mathbf{H_s^-}$ in the $z < 0$ region and $\mathbf{E_s^+}, \mathbf{H_s^+}$ in the $z > 0$ region. Hence, the total fields for $z < 0$ can be written as

$$\mathbf{E_t^-} = \mathbf{E_i} + \mathbf{E_s^-}, \qquad \mathbf{H_t^-} = \mathbf{H_i} + \mathbf{H_s^-} \tag{2.1}$$

and for $z > 0$

$$\mathbf{E_t^+} = \mathbf{E_i} + \mathbf{E_s^+}, \qquad \mathbf{H_t^+} = \mathbf{H_i} + \mathbf{H_s^+} \tag{2.2}$$

The far field in (2.2) consists mainly of the scattered fields $\mathbf{E_s}, \mathbf{H_s}$ since the incident fields $\mathbf{E_i}, \mathbf{H_i}$ do not contribute to the far field radiation. Hence, the far field radiation can be determined by finding the total scattered fields due to the rod/cone geometry. These fields are evaluated by decomposing the rod/cone structure into two separate

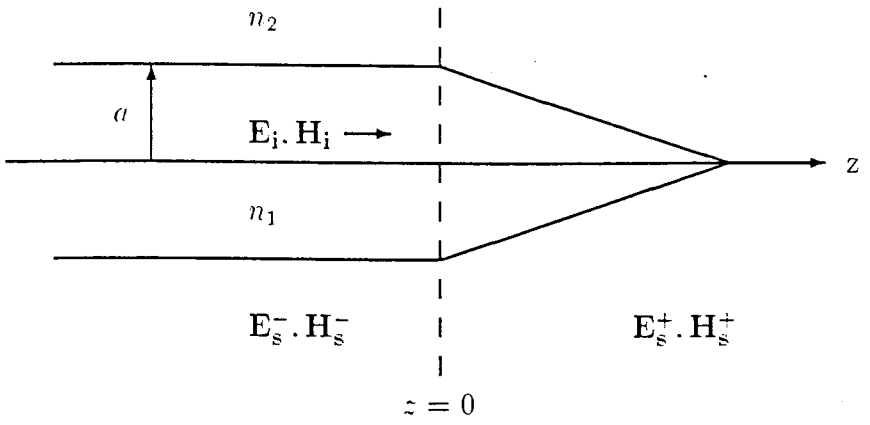

Figure 2.1 Tapered uniform cylindrical dielectric rod/cone geometry.

regions as shown in Fig.2.2 . and then using fictitious equivalent surface and volume currents as sources to account for the scattered fields in the $z > 0$ region.

In Fig.2.2(a). let the fields be for $z < 0$.

$$\mathbf{E_a^-} = \mathbf{E_i}. \quad \mathbf{H_a^-} = \mathbf{H_i} \tag{2.3}$$

and for $z > 0$

$$\mathbf{E_a^+} = 0. \quad \mathbf{H_a^+} = 0 \tag{2.4}$$

To support these fields the *surface equivalence* theorem. introduced by Schelkunoff. states that there may exist fictitious electric and magnetic *surface current densities* $\mathbf{J_s}$ and $\mathbf{M_s}$ on the $z = 0$ plane such that:

$$\mathbf{J_s} = \hat{\mathbf{n}} \times (\mathbf{H_a^+} - \mathbf{H_a^-}) = -\hat{\mathbf{z}} \times \mathbf{H_i} \tag{2.5}$$

$$\mathbf{M_s} = -\hat{\mathbf{n}} \times (\mathbf{E_a^+} - \mathbf{E_a^-}) = \hat{\mathbf{z}} \times \mathbf{E_i} \tag{2.6}$$

The total fields must equal the superposition of the fields in Fig.2.2(a) and 2.2(b). Therefore, the fields in Fig.2.2(b) are given by:

$$\mathbf{E_b^-} = \mathbf{E_t^-} - \mathbf{E_i} = \mathbf{E_s^-}, \quad \mathbf{H_b^-} = \mathbf{H_t^-} - \mathbf{H_i} = \mathbf{H_s^-} \tag{2.7}$$

for $z < 0$. and

$$\mathbf{E_b^+} = \mathbf{E_t^+} - 0 = \mathbf{E_s^+} + \mathbf{E_i}, \quad \mathbf{H_b^+} = \mathbf{H_t^+} - 0 = \mathbf{H_s^+} + \mathbf{H_i} \tag{2.8}$$

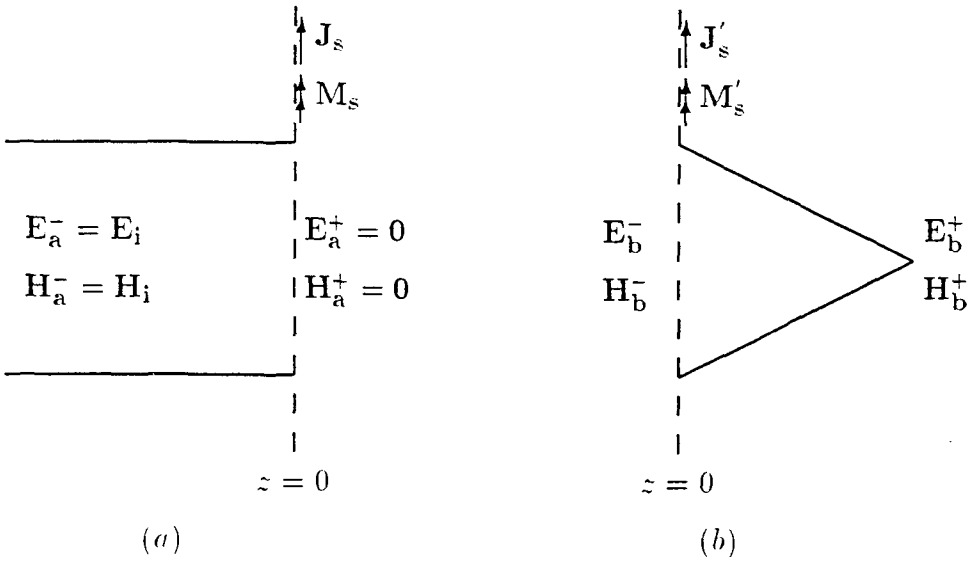

Figure 2.2 Decomposition of the dielectric rod/cone structure: (a) The dielectric rod in the $z < 0$ region. (b) The tapered dielectric in the $z > 0$ region.

for $z > 0$. Again according to the *surface equivalence* theorem, these fields yield fictitious *surface current densities* $\mathbf{J}_s'$ and $\mathbf{M}_s'$ in the $z = 0$ plane. The superposition of the fictitious surface currents in Figs.2.2(a) and 2.2(b) must produce a null field. Hence,

$$\mathbf{J}_s^t = \mathbf{J}_s + \mathbf{J}_s' = 0 \Longrightarrow \mathbf{J}_s' = -\mathbf{J}_s \tag{2.9}$$

$$\mathbf{M}_s^t = \mathbf{M}_s + \mathbf{M}_s' = 0 \Longrightarrow \mathbf{M}_s' = -\mathbf{M}_s \tag{2.10}$$

Thus for Fig.2.2(b) the equivalent surface currents are

$$\mathbf{J}_s' = \hat{z} \times \mathbf{H}_i, \quad \mathbf{M}_s' = -\hat{z} \times \mathbf{E}_i \tag{2.11}$$

which are known. From $\mathbf{J}_s'$ and $\mathbf{M}_s'$ the unknown fields $\mathbf{E}_s$ and $\mathbf{H}_s$ can be evaluated.

The equivalent surface currents $\mathbf{J}_s'$ and $\mathbf{M}_s'$ account for only a part of the total scattered field. The remaining scattered field is due to the unknown field $\mathbf{E}_c$ in the cone as depicted in Fig.2.3(a). This scattered field can now be found by introducing an equivalent electric *volume current density* $\mathbf{J}_v$ as seen in Fig.2.3(b). The equivalent volume current $\mathbf{J}_v$ "exists" only within the space previously occupied by the

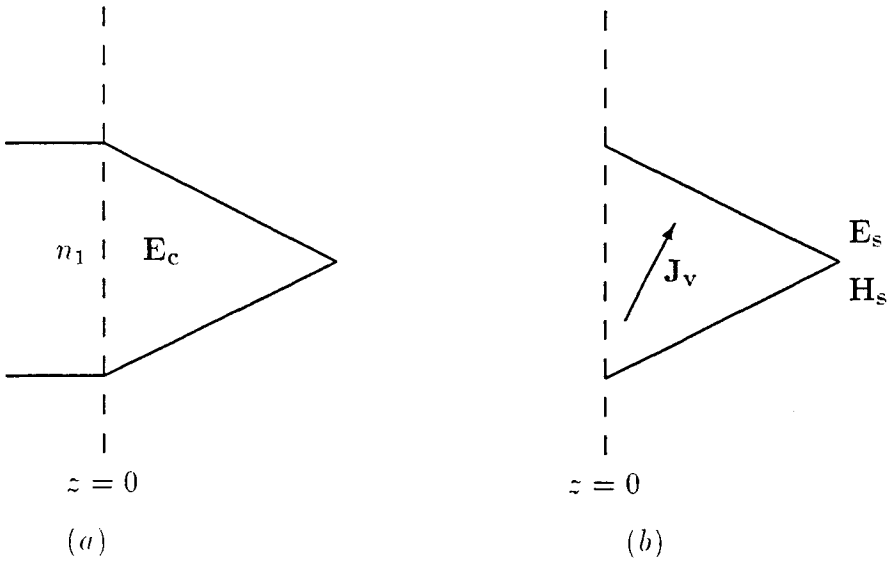

Figure 2.3 The dielectric cone: (a) Actual problem. (b) Volume equivalence model.

dielectric cone where it radiates into a free-space environment. By manipulating Maxwell's equations, valid within the dielectric cone, it can be shown that

$$\nabla \times \mathbf{E_s} = -j\omega\epsilon_2\mathbf{H_s} \tag{2.12}$$

$$\nabla \times \mathbf{H_s} = \mathbf{J_v} + j\omega\epsilon_2\mathbf{E_s} \tag{2.13}$$

where

$$\mathbf{J_v} = j\omega\epsilon_2(n_1^2 - 1)\mathbf{E_c} \tag{2.14}$$

and where $\mathbf{E_c}$ is the unknown E-field within the dielectric cone. However, $\mathbf{E_c}$ which is dependant on the radius of the cone, can be determined using the *local mode theory* and the principle of *power conservation*.

CHAPTER 3

THE CYLINDRICAL DIELECTRIC WAVEGUIDE

The problem of electromagnetic waves propagating along a perfect dielectric cylinder of infinite length embedded in an infinite and homogeneous medium has a well known exact analytical solution [2]. The general modal field solutions to Maxwell's equations are obtained under the appropriate boundary conditions to yield the eigenvalue equation for determining the modal propagation constant. The mode properties and the modal power flow for the fundamental HE_{11} [5] mode and the succeeding TE_{01} mode are derived below.

3.1 Modal Field Solutions of the Cylindrical Waveguide

A perfectly cylindrical dielectric waveguide of infinite length is shown in Fig.3.1(a). It consists of a rod of uniform refractive index n_1 and radius a surrounded by a medium of refractive index n_2, the refractive index profile being as shown in Fig.3.1(b).

Assume that the time harmonic fields have the form $\Psi(x, y, z)e^{j\omega t}$ where Ψ represents the **E**- or **H**-field. The time dependence for all the field components is of the form $e^{j\omega t}$. The time harmonic form of *Maxwell's equations* in a source free linear isotropic medium leads to

$$\nabla^2\Psi + k^2\Psi = 0 \tag{3.1}$$

where $k^2 = \omega^2\mu_0\epsilon$. The parameter ϵ is the permittivity ($\epsilon = n^2\epsilon_0$) of the medium which experiences a step discontinuity at $\rho = a$ where n changes between n_1 and n_2. The parameter μ is the permeability of the medium and since both the rod and the medium are considered to be non-magnetic, $\mu = \mu_0$ in both regions.

By expanding the vector wave equation (3.1) in cylindrical coordinates (ρ, ϕ, z) and reducing it to three scalar wave equations for the $\hat{\rho}, \hat{\phi}$, and $\hat{z}$ components, it

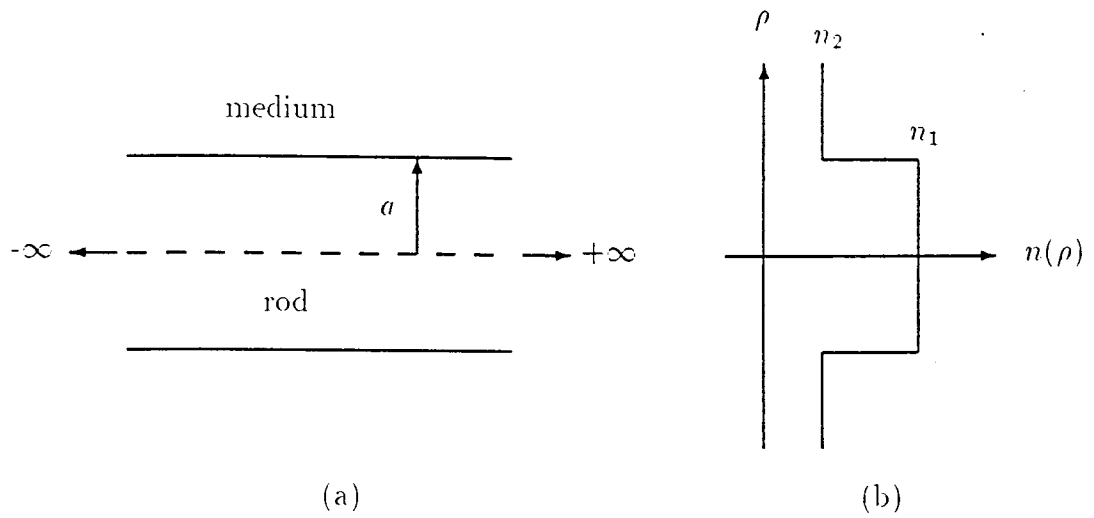

Figure 3.1 (a) Infinitely long uniform cylindrical rod waveguide (b) Refractive index profile.

yields

$$\nabla^2 v_\rho - \frac{2}{\rho^2}\frac{\partial v_\phi}{\partial \phi} + \left(k^2 - \frac{1}{\rho^2}\right) v_\rho = 0 \tag{3.2}$$

$$\nabla^2 v_\phi + \frac{2}{\rho^2}\frac{\partial v_\rho}{\partial \phi} + \left(k^2 - \frac{1}{\rho^2}\right) v_\phi = 0 \tag{3.3}$$

$$\nabla^2 v_z + k^2 v_z = 0 \tag{3.4}$$

where

$$\nabla^2 v_i = \frac{\partial^2 v_i}{\partial \rho^2} + \frac{1}{\rho}\frac{\partial v_i}{\partial \rho} + \frac{1}{\rho^2}\frac{\partial^2 v_i}{\partial \phi^2} + \frac{\partial^2 v_i}{\partial z^2} \quad , \qquad i = \rho, \phi, z$$

These equations are *uncoupled* second-order partial differential equations which can be solved analytically for the geometry shown in Fig.3.1

Assume fields of the form

$$\mathbf{E}(\rho, \phi, z) = \mathbf{E_0}(\rho, \phi)\epsilon^{-j\beta z}$$

$$\mathbf{H}(\rho, \phi, z) = \mathbf{H_0}(\rho, \phi)\epsilon^{-j\beta z} \tag{3.5}$$

where the term $\epsilon^{-j\beta z}$ represents a mode propagating in the $+z$ direction. The propagation constant β is the z component of the vector wavenumber, and will be determined from the eigenvalue equation.

By substituting the assumed fields of (3.5) into Maxwell's equations, the transverse field components E_ρ, E_ϕ, H_ρ, and H_ϕ can be expressed in terms of the longitudinal fields E_z and H_z:

$$E_\rho = -\frac{j}{q_i^2}\left(\beta\frac{\partial E_z}{\partial \rho} + \frac{\omega\mu_0}{\rho}\frac{\partial H_z}{\partial \phi}\right) \tag{3.6}$$

$$E_\phi = -\frac{j}{q_i^2}\left(\frac{\beta}{\rho}\frac{\partial E_z}{\partial \phi} - \omega\mu_0\frac{\partial H_z}{\partial \rho}\right) \tag{3.7}$$

$$H_\rho = -\frac{j}{q_i^2}\left(\beta\frac{\partial H_z}{\partial \rho} - \frac{\omega\epsilon}{\rho}\frac{\partial E_z}{\partial \phi}\right) \tag{3.8}$$

$$H_\phi = -\frac{j}{q_i^2}\left(\frac{\beta}{\rho}\frac{\partial H_z}{\partial \phi} + \omega\epsilon\frac{\partial E_z}{\partial \rho}\right) \tag{3.9}$$

where i can take the value of 1 or 2.

$$q_1^2 = \omega^2\mu_0\epsilon_1 - \beta^2 = k_1^2 - \beta^2 = u^2, \rho \le a \tag{3.10}$$

and,

$$q_2^2 = \omega^2\mu_0\epsilon_2 - \beta^2 = k_2^2 - \beta^2 = -w^2, \rho \ge a \tag{3.11}$$

By substituting the $\hat{z}$ component of (3.5) into (3.4) we get

$$\frac{\partial^2 v_z}{\partial \rho^2} + \frac{1}{\rho}\frac{\partial v_z}{\partial \rho} + \frac{1}{\rho^2}\frac{\partial^2 v_z}{\partial \phi^2} + q^2 v_z = 0 \tag{3.12}$$

which is then solved by the method of separation of variables. The solutions adopted here follow Snyder's notation [2] for the azimuthal variations, incorporating both even and odd modes: for $\rho \le a$,

$$E_{z1} = E_{rod}J_\nu(u\rho)f_\nu(\phi)\epsilon^{-j\beta z} \tag{3.13}$$

$$H_{z1} = H_{rod}J_\nu(u\rho)g_\nu(\phi)\epsilon^{-j\beta z} \tag{3.14}$$

and, for $\rho \ge a$,

$$E_{z2} = E_{med}K_\nu(w\rho)f_\nu(\phi)\epsilon^{-j\beta z} \tag{3.15}$$

$$H_{z2} = H_{med}K_\nu(w\rho)g_\nu(\phi)\epsilon^{-j\beta z} \tag{3.16}$$

where.

$$f_\nu(\phi) = \begin{cases} \cos\nu\phi & \text{for } even \text{ modes} \\ \sin\nu\phi & \text{for } odd \text{ modes} \end{cases} \tag{3.17}$$

$$g_\nu(\phi) = \begin{cases} \sin\nu\phi & \text{for } even \text{ modes} \\ -\cos\nu\phi & \text{for } odd \text{ modes} \end{cases} \tag{3.18}$$

In the above equations. the azimuthal index ν has to be an integer ($\nu = 0.1.2.3....$) for $f_\nu(\phi)$ and $g_\nu(\phi)$ to be angular periodic solutions. Furthermore in order to have finite fields at the rod axis ($\rho = 0$). *Bessel functions of the First Kind.* $J_\nu(u\rho)$. are chosen for the rod region ($\rho \leq a$). In the surrounding medium ($\rho \geq a$). *Modified Bessel functions of the Second Kind.* $K_\nu(w\rho)$. are chosen because they exhibit the desired evanescent behavior.

By substituting (3.14) and (3.16) into (3.9) the transverse fields can be written as:

$$E_{\rho 1} = -\frac{j}{u}\left(\beta E_{rod} J_\nu'(u\rho) + \frac{\omega\mu_0\nu}{u\rho} H_{rod} J_\nu(u\rho)\right) f_\nu(\phi)\epsilon^{-j\beta z} \tag{3.19}$$

$$E_{\phi 1} = \frac{j}{u}\left(\frac{\beta\nu}{u\rho} E_{rod} J_\nu(u\rho) + \omega\mu_0 H_{rod} J_\nu'(u\rho)\right) g_\nu(\phi)\epsilon^{-j\beta z} \tag{3.20}$$

$$H_{\rho 1} = -\frac{j}{u}\left(\beta H_{rod} J_\nu'(u\rho) + \frac{\omega\epsilon_1\nu}{u\rho} E_{rod} J_\nu(u\rho)\right) g_\nu(\phi)\epsilon^{-j\beta z} \tag{3.21}$$

$$H_{\phi 1} = -\frac{j}{u}\left(\frac{\beta\nu}{u\rho} H_{rod} J_\nu(u\rho) + \omega\epsilon_1 E_{rod} J_\nu'(u\rho)\right) f_\nu(\phi)\epsilon^{-j\beta z} \tag{3.22}$$

for $\rho \leq a$. and

$$E_{\rho 2} = \frac{j}{w}\left(\beta E_{med} K_\nu'(w\rho) + \frac{\omega\mu_0\nu}{w\rho} H_{med} K_\nu(w\rho)\right) f_\nu(\phi)\epsilon^{-j\beta z} \tag{3.23}$$

$$E_{\phi 2} = -\frac{j}{w}\left(\frac{\beta\nu}{w\rho} E_{med} K_\nu(w\rho) + \omega\mu_0 H_{med} K_\nu'(w\rho)\right) g_\nu(\phi)\epsilon^{-j\beta z} \tag{3.24}$$

$$H_{\rho 2} = \frac{j}{w}\left(\beta H_{med} K_\nu'(w\rho) + \frac{\omega\epsilon_2\nu}{w\rho} E_{med} K_\nu(w\rho)\right) g_\nu(\phi)\epsilon^{-j\beta z} \tag{3.25}$$

$$H_{\phi 2} = \frac{j}{w}\left(\frac{\beta\nu}{w\rho} H_{med} K_\nu(w\rho) + \omega\epsilon_2 E_{med} K_\nu'(w\rho)\right) f_\nu(\phi)\epsilon^{-j\beta z} \tag{3.26}$$

for $\rho \geq a$. The primed Bessel functions indicate differentiation with respect to their arguments.

3.2 General Eigenvalue Equations

The boundary condition of a cylindrical dielectric waveguide demands that all the tangential field components be continuous over the boundary at $\rho = a$. These four boundary conditions are

$$E_{z1} = E_{z2}$$

$$E_{\phi 1} = E_{\phi 2}$$

$$H_{z1} = H_{z2}$$

$$H_{\phi 1} = H_{\phi 2} \tag{3.27}$$

where the subscripts 1 and 2 represent the rod and the medium, respectively. Substitution of the tangential field components in (3.22) and (3.26) into (3.27) at $\rho = a$ result in a set of four equations, with four unknown coefficients E_{rod}, E_{med}, H_{rod} and H_{med}. The non-trivial solutions of this set of linear equations are as follows:

$$E_{med} = \frac{J_\nu(U)}{K_\nu(W)} E_{rod} \tag{3.28}$$

$$H_{rod} = -\frac{\beta\nu\left(\frac{V}{UW}\right)^2}{\omega\mu_0\left(F_\nu(U) + G_\nu(W)\right)} E_{rod} = Y_\nu E_{rod} \tag{3.29}$$

$$H_{med} = \frac{J_\nu(U)}{K_\nu(W)} H_{rod} = \frac{J_\nu(U)}{K_\nu(W)} Y_\nu E_{rod} \tag{3.30}$$

where Y_ν= wave admittance, and the eigenvalue equation [2] for the $HE_{\nu m}$ and $EH_{\nu m}$ modes ($\nu \geq 1$):

$$\left(F_\nu(U) + G_\nu(W)\right)\left(F_\nu(U) + \frac{n_2^2}{n_1^2} G_\nu(W)\right) = \left(\frac{\beta\nu}{k_1}\right)^2 \left(\frac{V}{UW}\right)^4 \tag{3.31}$$

for TE_{0m} modes ($\nu = 0$):

$$F_0(U) + G_0(W) = 0 \tag{3.32}$$

and finally for TM_{0m} modes ($\nu = 0$):

$$F_0(U) + \frac{n_2^2}{n_1^2} G_0(W) = 0 \tag{3.33}$$

where

$$F_\nu(U) = \frac{J'_\nu(U)}{UJ_\nu(U)}, \qquad G_\nu(W) = \frac{K'_\nu(W)}{WK_\nu(W)} \tag{3.34}$$

$$U = ua = a\sqrt{k_1^2 - \beta^2} \tag{3.35}$$

$$W = wa = a\sqrt{\beta^2 - k_2^2} \tag{3.36}$$

$$V = \sqrt{U^2 + W^2} = \frac{2\pi a}{\lambda}\sqrt{n_1^2 - n_2^2} = \text{ Normalized Frequency} \tag{3.37}$$

$$k = \frac{2\pi}{\lambda}. \quad k_1 = kn_1. \quad k_2 = kn_2 \tag{3.38}$$

The eigenvalue equations (3.31) to (3.33) are complicated transcendental equations and must be solved numerically or graphically.

The hybrid $HE_{\nu m}$ and $EH_{\nu m}$ are twofold degenerate (even and odd) modes consisting of all six field components and without any circular symmetry. The dominant longitudinal field component E_z or H_z determines the designation EH or HE, respectively. The only circular symmetric modes are the TE and TM modes ($\nu = 0$). Each mode is labeled by two subscripts. The first subscript ν is the order, while the second subscript m denotes the m^{th} root of the eigenvalue equation. The roots are ordered so that $m = 1$ corresponds to the root with the smallest value of U for a given value of ν. The values of β for all bound modes take only discrete values within the range

$$k_2 < \beta \leq k_1 \tag{3.39}$$

and the solution of the eigenvalue equation for any particular mode completely characterizes the mode.

The recurrence relations for the *Bessel functions* are given by [6]:

$$J'_\nu(z) = J_{\nu-1} - \frac{\nu}{z}J_\nu(z) K'_\nu(z) = -K_{\nu-1} - \frac{\nu}{z}K_\nu(z) \tag{3.40}$$

By substituting (3.28-3.30) into (3.22) and (3.26) and by using the above recurrence relations the modal field solutions with only one unknown excitation coefficient E_{rod}

take the final form [5]:

$$E_{\rho 1} = -\frac{jE_{rod}}{u}\left[\beta J_{\nu-1}(u\rho) + \frac{\nu(\omega\mu_0 Y_\nu - \beta)}{u\rho}J_\nu(u\rho)\right] f_\nu(\phi)\epsilon^{-j\beta z} \quad (3.41)$$

$$E_{\phi 1} = \frac{jE_{rod}}{u}\left[\omega\mu_0 Y_\nu J_{\nu-1}(u\rho) + \frac{\nu(\beta - \omega\mu_0 Y_\nu)}{u\rho}J_\nu(u\rho)\right] g_\nu(\phi)\epsilon^{-j\beta z} \quad (3.42)$$

$$E_{z1} = E_{rod}J_\nu(u\rho) f_\nu(\phi)\epsilon^{-j\beta z} \quad (3.43)$$

$$H_{\rho 1} = -\frac{jE_{rod}}{u}\left[\beta Y_\nu J_{\nu-1}(u\rho) + \frac{\nu(\omega\epsilon_1 - \beta Y_\nu)}{u\rho}J_\nu(u\rho)\right] g_\nu(\phi)\epsilon^{-j\beta z} \quad (3.44)$$

$$H_{\phi 1} = -\frac{jE_{rod}}{u}\left[\omega\epsilon_1 J_{\nu-1}(u\rho) + \frac{\nu(\beta Y_\nu - \omega\epsilon_1)}{u\rho}J_\nu(u\rho)\right] f_\nu(\phi)\epsilon^{-j\beta z} \quad (3.45)$$

$$H_{z1} = Y_\nu E_{rod}J_\nu(u\rho) g_\nu(\phi)\epsilon^{-j\beta z} \quad (3.46)$$

for $\rho \leq a$. and

$$E_{\rho 2} = -\frac{jE_{rod}}{w}\frac{J_\nu(U)}{K_\nu(W)}\left[\beta K_{\nu-1}(w\rho) + \frac{\nu(\beta - \omega\mu Y_\nu)}{w\rho}K_\nu(w\rho)\right] f_\nu(\phi)\epsilon^{-j\beta z} \quad (3.47)$$

$$E_{\phi 2} = \frac{jE_{rod}}{w}\frac{J_\nu(U)}{K_\nu(W)}\left[\omega\mu_0 Y_\nu K_{\nu-1}(w\rho) + \frac{\nu(\omega\mu_0 Y_\nu - \beta)}{w\rho}K_\nu(w\rho)\right] g_\nu(\phi)\epsilon^{-j\beta z} \quad (3.48)$$

$$E_{z2} = E_{rod}\frac{J_\nu(U)}{K_\nu(W)}K_\nu(w\rho) f_\nu(\phi)\epsilon^{-j\beta z} \quad (3.49)$$

$$H_{\rho 2} = -\frac{jE_{rod}}{w}\frac{J_\nu(U)}{K_\nu(W)}\left[\beta Y_\nu K_{\nu-1}(w\rho) + \frac{\nu(\beta Y_\nu - \omega\epsilon_2)}{w\rho}K_\nu(w\rho)\right] g_\nu(\phi)\epsilon^{-j\beta z} \quad (3.50)$$

$$H_{\phi 2} = -\frac{jE_{rod}}{w}\frac{J_\nu(U)}{K_\nu(W)}\left[\omega\epsilon_2 K_{\nu-1}(w\rho) + \frac{\nu(\omega\epsilon_2 - \beta Y_\nu)}{w\rho}K_\nu(w\rho)\right] f_\nu(\phi)\epsilon^{-j\beta z} \quad (3.51)$$

$$H_{z2} = Y_\nu E_{rod}\frac{J_\nu(U)}{K_\nu(W)}K_\nu(w\rho) g_\nu(\phi)\epsilon^{-j\beta z} \quad (3.52)$$

for $\rho \geq a$.

3.3 HE_{11} Modal Fields and Eigenvalues

By letting $\nu = 1$ in the general modal field solutions. the HE_{1m} and EH_{1m} modal fields are obtained [5]:

$$E_{\rho 1} = -\frac{jE_{rod}}{u}\left[\beta J_0(u\rho) + \frac{(\omega\mu_0 Y_1 - \beta)}{u\rho}J_1(u\rho)\right] f_1(\phi)\epsilon^{-j\beta z}$$

$$E_{\phi 1} = \frac{jE_{rod}}{u}\left[\omega\mu_0 Y_1 J_0(u\rho) + \frac{(\beta - \omega\mu_0 Y_1)}{u\rho}J_1(u\rho)\right] g_1(\phi)\epsilon^{-j\beta z}$$

$$E_{z1} = E_{rod}J_1(u\rho) f_1(\phi)\epsilon^{-j\beta z}$$

$$H_{\rho 1} = -\frac{jE_{rod}}{u}\left[\beta Y_1 J_0(u\rho) + \frac{(\omega\epsilon_1 - \beta Y_1)}{u\rho} J_1(u\rho)\right] g_1(\phi)\epsilon^{-j\beta z}$$

$$H_{\phi 1} = -\frac{jE_{rod}}{u}\left[\omega\epsilon_1 J_0(u\rho) + \frac{(\beta Y_1 - \omega\epsilon_1)}{u\rho} J_1(u\rho)\right] f_1(\phi)\epsilon^{-j\beta z}$$

$$H_{z1} = Y_1 E_{rod} J_1(u\rho) g_1(\phi)\epsilon^{-j\beta z} \tag{3.53}$$

for $\rho \leq a$. and

$$E_{\rho 2} = -\frac{jE_{rod}}{w}\frac{J_1(U)}{K_1(W)}\left[\beta K_0(w\rho) + \frac{(\beta - \omega\mu Y_1)}{w\rho} K_1(w\rho)\right] f_1(\phi)\epsilon^{-j\beta z}$$

$$E_{\phi 2} = \frac{jE_{rod}}{w}\frac{J_1(U)}{K_1(W)}\left[\omega\mu_0 Y_1 K_0(w\rho) + \frac{(\omega\mu_0 Y_1 - \beta)}{w\rho} K_1(w\rho)\right] g_1(\phi)\epsilon^{-j\beta z}$$

$$E_{z2} = E_{rod}\frac{J_1(U)}{K_1(W)} K_1(w\rho) f_1(\phi)\epsilon^{-j\beta z}$$

$$H_{\rho 2} = -\frac{jE_{rod}}{w}\frac{J_1(U)}{K_1(W)}\left[\beta Y_1 K_0(w\rho) + \frac{(\beta Y_1 - \omega\epsilon_2)}{w\rho} K_1(w\rho)\right] g_1(\phi)\epsilon^{-j\beta z}$$

$$H_{\phi 2} = -\frac{jE_{rod}}{w}\frac{J_1(U)}{K_1(W)}\left[\omega\epsilon_2 K_0(w\rho) + \frac{(\omega\epsilon_2 - \beta Y_1)}{w\rho} K_1(w\rho)\right] f_1(\phi)\epsilon^{-j\beta z}$$

$$H_{z2} = Y_1 E_{rod}\frac{J_1(U)}{K_1(W)} K_1(w\rho) g_1(\phi)\epsilon^{-j\beta z} \tag{3.54}$$

for $\rho \geq a$. where

$$f_1(\phi) = \begin{cases} \cos\phi & \text{for } even \text{ modes} \\ \sin\phi & \text{for } odd \text{ modes} \end{cases} \tag{3.55}$$

and

$$g_1(\phi) = \begin{cases} \sin\phi & \text{for } even \text{ modes} \\ -\cos\phi & \text{for } odd \text{ modes} \end{cases} \tag{3.56}$$

Furthermore, the HE_{1m} and EH_{1m} eigenvalue equation becomes:

$$\left(F_1(U) + G_1(W)\right)\left(F_1(U) + \frac{n_2^2}{n_1^2} G_1(W)\right) = \left(\frac{\beta}{k_1}\right)^2 \left(\frac{V}{UW}\right)^4 \tag{3.57}$$

where

$$F_1(U) = \frac{J_1'(U)}{UJ_1(U)}, \qquad G_1(W) = \frac{K_1'(W)}{WK_1(W)} \tag{3.58}$$

and

$$Y_1 = -\frac{\beta\left(\frac{V}{UW}\right)^2}{\omega\mu_0\left(F_1(U) + G_1(W)\right)} \tag{3.59}$$

The propagation constant β as determined by the eigenvalue equation (3.57) dictates the functional dependency of the HE_{1m} and EH_{1m} modes. The solution for the HE_{11} mode is obtained using the first root of the eigenvalue equation.

3.4 TE_{01} Modal Fields and Eigenvalues

The TE_{01} mode is circularly symmetric about the axis of the waveguide. A rigorous solution of *Maxwell's equations* for this mode yields the vanishing results for the $E_{\rho 1}, E_{\rho 2}, E_{z1}, E_{z2}, H_{\phi 1}$ and $H_{\phi 2}$ components. The only non-zero field components are E_ϕ, H_ρ and H_z [2].

In the rod i.e. for $\rho \leq a$

$$\begin{aligned} E_{\phi 1} &= \frac{-j}{u} J_1(u\rho)\omega\mu_0 H_{rod}\epsilon^{-j\beta z} \\ H_{\rho 1} &= \frac{j}{u} J_1(u\rho)\beta H_{rod}\epsilon^{-j\beta z} \\ H_{z1} &= J_0(u\rho)H_{rod}\epsilon^{-j\beta z} \end{aligned} \tag{3.60}$$

For $\rho \geq a$,

$$E_{\phi 2} = \frac{-j}{w} K_1(w\rho)\omega\mu_0 a H_{rod}\epsilon^{-j\beta z} \tag{3.61}$$

$$H_{\rho 2} = \frac{j}{w}\beta a K_1(w\rho)H_{rod}\epsilon^{-j\beta z} \tag{3.62}$$

$$H_{z2} = a K_0(w\rho)H_{rod}\epsilon^{-j\beta z} \tag{3.63}$$

The eigenvalue equation has the form

$$\frac{J_1(ua)}{uJ_0(ua)} = \frac{-K_1(wa)}{wK_0(wa)} \tag{3.64}$$

where, $u = \sqrt{k_1^2 - \beta^2}$ and $w = \sqrt{\beta^2 - k_2^2}$

3.5 Modal Power Flow

The power flow of a mode in the $+z$ direction is evaluated by integrating the z-component of the *Poynting vector* $\mathbf{S}$ over the cross-section:

$$P_{av} = \int_S \mathbf{S} \cdot \mathbf{ds} \tag{3.65}$$

where $\mathbf{S} = \frac{1}{2} R\epsilon(\mathbf{E} \times \mathbf{H}^*)$. and $\mathbf{ds} = \hat{\mathbf{z}}\, \rho d\rho d\phi$. The electromagnetic energy of a bound mode in a cylindrical dielectric waveguide is carried partly in the rod and partly in the surrounding medium. This is due to the fact that the transverse field components at the dielectric boundary $\rho = a$ are nonzero.

3.5.1 HE_{11} mode

Using the expressions for $E_{\rho 1}, E_{\rho 2}, E_{\phi 1}, E_{\phi 2}$, $H_{\rho 1}, H_{\rho 2}, H_{\phi 1}$ and $H_{\phi 2}$ from (3.53) and (3.54), we obtain the power flow for the HE_{11} mode in the rod [5] as

$$P_1 = \frac{1}{2} \int_0^a \int_0^{2\pi} R\epsilon(E_{\rho 1} H_{\phi 1}^* - E_{\phi 1} H_{\rho 1}^*) \rho d\phi d\rho \tag{3.66}$$

which leads to.

$$P_1 = \frac{\pi}{4} \left(\frac{E_{rod}}{u}\right)^2 \left[C_1 a^2 J_0^2(ua) + \left(C_1 a^2 - C_2\right) J_1^2(ua)\right] \tag{3.67}$$

while in the surrounding medium the power flow is given by

$$P_2 = \frac{1}{2} \int_a^\infty \int_0^{2\pi} R\epsilon(E_{\rho 2} H_{\phi 2}^* - E_{\phi 2} H_{\rho 2}^*) \rho d\phi d\rho \tag{3.68}$$

which results in.

$$P_2 = \frac{\pi}{4} \left[\frac{E_{rod} J_1(ua)}{w K_1(wa)}\right]^2 \left[\left(C_3 a^2 + C_4\right) K_1^2(wa) - C_3 a^2 K_0^2(wa)\right] \tag{3.69}$$

where.

$$C_1 = \omega\beta(\epsilon_1 + \mu_0 Y_1^2) \quad C_2 = \frac{2}{u^2}(\omega\epsilon_1 - \beta Y_1)(\beta - \omega\mu_0 Y_1)$$
$$C_3 = \omega\beta(\epsilon_2 + \mu_0 Y_1^2) \quad C_4 = \frac{2}{w^2}(\omega\epsilon_2 - \beta Y_1)(\beta - \omega\mu_0 Y_1)$$

Thus. the total power carried by the HE_{11} mode in the dielectric waveguide is given by:

$$P_{z<0} = \frac{\pi}{4} E_{rod}^2 \left\{ \frac{1}{u^2} \left[C_1 a^2 J_0^2(ua) + \left(C_1 a^2 - C_2\right) J_1^2(ua)\right] + \left[\frac{J_1(ua)}{w K_1(wa)}\right]^2 \left[\left(C_3 a^2 + C_4\right) K_1^2(wa) - C_3 a^2 K_0^2(wa)\right] \right\} \tag{3.70}$$

$$P_{z<0} = P_1 + P_2 = \frac{\pi}{4} E_{rod}^2 P_0 \tag{3.71}$$

3.5.2 TE_{01} mode

For the TE_{01} mode, the power in the rod and surrounding medium is obtained by substituting (3.60) to (3.63) into integral equations for power as above. In the rod,

$$P_1 = \frac{1}{2}\int_0^a \int_0^{2\pi} Re(-E_{\phi 1}H_{\rho 1}^*)\rho d\rho d\phi \tag{3.72}$$

After analytical evaluation, (3.72) yields

$$P_1 = \frac{\pi\omega\mu_0\beta a^2}{2u^2}H_{rod}^2\left[J_1^2(ua) - J_0(ua)J_2(ua)\right] \tag{3.73}$$

In the surrounding medium,

$$P_2 = \frac{1}{2}\int_a^\infty \int_0^{2\pi} Re(-E_{\phi 2}H_{\rho 2}^*)\rho d\rho d\phi \tag{3.74}$$

which reduces it to,

$$P_2 = \frac{-\pi\omega\mu_0\beta\alpha^2 a^2}{2w^2}H_{rod}^2\left[K_1^2(wa) - K_0(wa)K_2(wa)\right] \tag{3.75}$$

where $\alpha = \frac{J_0(ua)}{K_0(wa)}$. In order to evaluate the integrals leading to the above equations, the following integral properties of *Bessel functions* were used [6]

$$\begin{aligned}\int zJ_m^2(az)dz &= \frac{z^2}{2}\left[J_m^2(az) - J_{m-1}(az)J_{m+1}(az)\right]\\ \int zK_m^2(az)dz &= \frac{z^2}{2}\left[K_m^2(az) - K_{m-1}(az)K_{m+1}(az)\right]\end{aligned} \tag{3.76}$$

The total power carried by the TE_{01} mode in the dielectric waveguide is then given by

$$\begin{aligned}P_{z<0} = P_1 + P_2 = \frac{\pi\omega\mu_0\beta a^2 H_{rod}^2}{2}\Bigg[&\frac{1}{u^2}\Big(J_1^2(ua) - J_0(ua)J_2(ua)\Big)\\ &-\frac{\alpha^2}{w^2}\Big(K_1^2(wa) - K_0(wa)K_2(wa)\Big)\Bigg]\end{aligned} \tag{3.77}$$

CHAPTER 4

THE DIELECTRIC TAPER

In the case of a slow change in the profile of the dielectric rod, it is possible to use the results obtained in Chapter 2 to approximately evaluate the modal field solutions of Maxwell's equations within local regions [2]. These *local modes* are governed by the local field solutions and the principle of *conservation of power*. Since such a solution assumes a negligible change in the power of the local mode, it is often called the *adiabatic approximation*.

4.1 Local Mode Field Solutions

The local mode field solutions are constructed by approximating the dielectric cone by a series of cylindrical sections as shown in Fig. 4.1. The profile is independent of z within each section and is defined at the center $z = z_c$. The local mode field solutions within each *finite* section are approximated by the modal fields of an *infinitely* long rod having radius $a(z)$ equal to the radius at the center of the section. Assuming that the length of the section δz is large compared to the length scale of the fields within δz, such an approximation is fairly accurate.

As a local mode propagates, its phase increases across each section by the product of $\beta(z_c)$ and the section length δz. Consequently, the phase at an arbitrary position along the nonuniform dielectric rod is the sum of such products. However, the slow variation of the dielectric rod means that the propagation constant $\beta(z_c)$ varies only slightly between adjacent sections. Hence the sum of the phase contributions from each section can be approximated by [2].

$$\sum_{i=1}^{n} \beta(z_c)\delta z = \int_0^z \beta(\xi)d\xi \tag{4.1}$$

where ξ is a dummy variable. The local mode fields in the conical structure for the HE_{11} mode can thus be obtained by replacing the phase term in (3.53) by the above

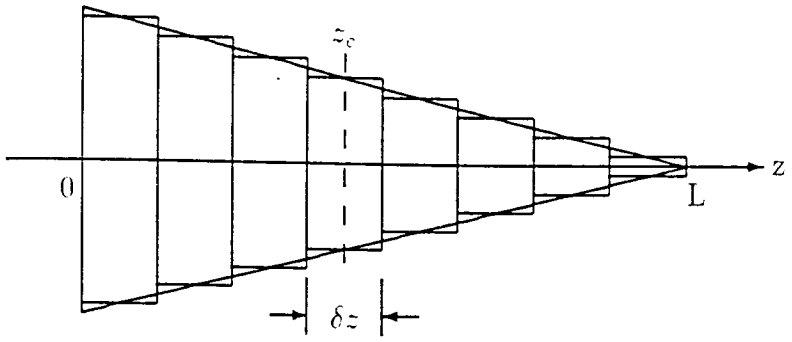

Figure 4.1 The approximate model for the dielectric cone.

integral [5]:

$$
\begin{aligned}
E_{\rho 1} &= -\frac{jE_{rod}(z)}{u(z)}\left[\beta(z)J_0(\gamma) + \frac{(\omega\mu_0)Y_1(z) - \beta(z))}{u(z)\rho(z)}J_1(\gamma)\right] f_1(o)\epsilon^{-j\int_0^z \beta(\xi)d\xi} \\
E_{\phi 1} &= \frac{jE_{rod}(z)}{u(z)}\left[\omega\mu_0 Y_1(z)J_0(\gamma) + \frac{(\beta(z) - \omega\mu_0)Y_1(z))}{u(z)\rho(z)}J_1(\gamma)\right] g_1(o)\epsilon^{-j\int_0^z \beta(\xi)d\xi} \\
E_{z1} &= E_{rod}(z)J_1(\gamma)f_1(o)\epsilon^{-j\int_0^z \beta(\xi)d\xi} \\
H_{\rho 1} &= -\frac{jE_{rod}(z)}{u(z)}\left[\beta(z)Y_1(z)J_0(\gamma) + \frac{(\omega\epsilon_1 - \beta(z))Y_1(z))}{u(z)\rho(z)}J_1(\gamma)\right] g_1(o)\epsilon^{-j\int_0^z \beta(\xi)d\xi} \\
H_{\phi 1} &= -\frac{jE_{rod}(z)}{u(z)}\left[\omega\epsilon_1 J_0(\gamma) + \frac{(\beta(z)Y_1(z) - \omega\epsilon_1)}{u(z)\rho(z)}J_1(\gamma)\right] f_1(o)\epsilon^{-j\int_0^z \beta(\xi)d\xi} \\
H_{z1} &= Y_1(z)E_{rod}(z)J_1(\gamma)g_1(o)\epsilon^{-j\int_0^z \beta(\xi)d\xi}
\end{aligned}
\tag{4.2}
$$

where $\gamma = u(z)\rho(z)$, while E_{rod}, β, u and Y_1 all become functions of z since they are directly related to the radius $a(z)$ which is a linear function of z in the conical region. The amplitude of the fields within the conical dielectric taper, $E_{rod}(z)$ is to be determined by the principle of *conservation of power*.

Similarly, the local fields for the TE_{01} mode are determined by substituting (4.1) into (3.60) to give

$$
\begin{aligned}
E_{\phi 1} &= \frac{-j}{u(z)}J_1(u(z)\rho(z))\omega\mu_0 H_{rod}(z)\epsilon^{-j\int_0^z \beta(\xi)d\xi} \\
H_{\rho 1} &= \frac{j}{u(z)}J_1(u(z)\rho(z))\beta(z)H_{rod}\epsilon^{-j\int_0^z \beta(\xi)d\xi} \\
H_{z1} &= J_0(u(z)\rho(z))H_{rod}(z)\epsilon^{-j\int_0^z \beta(\xi)d\xi}
\end{aligned}
\tag{4.3}
$$

Again, the amplitude term $H_{rod}(z)$ is to be determined using power conservation.

4.2 Power Conservation

The local mode fields derived in the previous section are very accurate approximations to Maxwell's equations in *slowly* varying waveguides. However since it is not an exact solution, the local mode will suffer some loss of power as it propagates along the conical region. This loss of power can be attributed to coupling to radiation modes and higher order local modes. Even though the fields expressed by (4.2) and (4.3) vary as the radius $a(z)$ varies from section to section, the power of the local mode must be conserved along the dielectric rod/cone structure. This principle of *power conservation* can be expressed as

$$P_{z<0} = P_{z>0} \tag{4.4}$$

where $P_{z<0}$ is the total average power carried by the mode in the uniform cylindrical dielectric waveguide as given by (3.70) for the HE_{11} mode and (3.77) for the TE_{01} mode. The power flow in the tapered region, represented by $P_{z>0}$ for the HE_{11} mode is [5]:

$$P_{z>0} = \frac{\pi}{4} E_{rod}^2(z) \left\{ \frac{1}{u^2(z)} \left[C_1(z) a^2(z) J_0^2(\gamma_a) + \Big(C_1(z) a^2(z) - C_2(z) \Big) J_1^2(\gamma_a) \right] + \left[\frac{J_1(\gamma_a)}{w(z) K_1(\zeta_a)} \right]^2 \left[\Big(C_3(z) a^2(z) + C_4(z) \Big) K_1^2(\zeta_a) - C_3(z) a^2(z) K_0^2(\zeta_a) \right] \right\} \tag{4.5}$$

where $\gamma_a = u(z)a(z)$ and $\zeta_a = w(z)a(z)$, while the parameters u, w, C_1, C_2, C_3 and C_4 are also shown to be functions of z since they all change as the profile changes.

In the case of the TE_{01} mode, a similar evaluation yields,

$$P_{z>0} = \frac{\pi \omega \mu_0 \beta(z) a^2(z) H_{rod}^2(z)}{2} \left[\frac{1}{u^2(z)} \Big(J_1^2(u(z)a(z)) - J_0(u(z)a(z)) J_2(u(z)a(z)) \Big) - \frac{a^2(z)}{w^2(z)} \Big(K_1^2(w(z)a(z)) - K_0(w(z)a(z)) K_2(w(z)a(z)) \Big) \right] \tag{4.6}$$

By substituting the (3.70) and (4.5), and then (3.77) and (4.6) for the power flow, in the rod and cone respectively into (4.4), the following relationships between $E_{rod}(z).E_{rod}$ [5] and $H_{rod}(z).H_{rod}$ are obtained:

$$| E_{rod}(z) | = | E_{rod} | \sqrt{\frac{P_0}{P_0(z)}} \tag{4.7}$$

$$| H_{rod}(z) | = | H_{rod} | \sqrt{\frac{P_0}{P_0(z)}} \tag{4.8}$$

where $| E_{rod} |$ and $| H_{rod} |$ are the constant field amplitudes in the dielectric rod. In order to simplify further calculations, the unknown excitation coefficients are chosen so as to normalize the directive gain to unity (0 dB) at the maximum of the main radiation lobe.

CHAPTER 5

FAR FIELD RADIATION

The far fields generated by the rod/cone structure of the dielectric can be evaluated as a combination of surface and volume current densities as formulated in Chapter 2. $\mathbf{J}_s'$ and $\mathbf{M}_s'$ introduced in (2.11) and $\mathbf{J}_v$ introduced in (2.14) represent the surface and volume current densities, respectively. The radiation due to these equivalent current densities is expressed in terms of *magnetic* and *electric vector potentials* $\mathbf{A}(\mathbf{r})$ and $\mathbf{F}(\mathbf{r})$ defined as [7]

$$\mathbf{H} = \nabla \times \mathbf{A} \qquad \text{and} \qquad \mathbf{E} = -\nabla \times \mathbf{F} \tag{5.1}$$

While considering the far field radiation, the equivalent sources $\mathbf{J}_s'$, $\mathbf{M}_s'$ and $\mathbf{J}_v$ can be considered as radiating spherical waves in the outward $\hat{r}$ direction. These fields are TEM to r. The magnetic far field is related to the electric field by:

$$\mathbf{H} = \frac{1}{\eta_0}\hat{\mathbf{r}} \times \mathbf{E} = \frac{1}{\eta_0}\hat{\mathbf{r}} \times \left(\hat{\theta}E_\theta + \hat{o}E_o\right) = -\hat{\theta}\frac{E_o}{\eta_0} + \hat{o}\frac{E_\theta}{\eta_0} \tag{5.2}$$

where $\eta_0 = \sqrt{\mu_0/\epsilon_0}$ is the intrinsic impedance in free space. The total electric far fields are expressed in terms of the rectangular components of the vector potentials $\mathbf{A}(\mathbf{r})$ and $\mathbf{F}(\mathbf{r})$ as [7]

$$\begin{aligned} E_\theta^{ff} &= -j\omega\mu(\cos\theta\cos o A_x + \cos\theta\sin o A_y - \sin\theta A_z) - jk_0(-\sin o F_x + \cos o F_y) \\ E_o^{ff} &= -j\omega\mu(-\sin o A_x + \cos o A_y) + jk_0(\cos\theta\cos o F_x + \cos\theta\sin o F_y - \sin\theta F_z) \end{aligned} \tag{5.3}$$

where

$$\begin{aligned} A_i &= \frac{\epsilon^{-jk_0 r}}{4\pi r}\int\int\int_{source} J_i(r')\epsilon^{jk_0(\rho'\sin\theta\cos(\phi-\phi')+z'\cos\theta)}\rho'\,d\rho'\,d\phi'\,dz' \\ F_i &= \frac{\epsilon^{-jk_0 r}}{4\pi r}\int\int\int_{source} M_i(r')\epsilon^{jk_0(\rho'\sin\theta\cos(\phi-\phi')+z'\cos\theta)}\rho'\,d\rho'\,d\phi'\,dz' \end{aligned} \tag{5.4}$$

and where the prime denotes the source coordinates, r the distance from the origin to the observation point, and i denotes any of the rectangular coordinates x, y, z.

5.1 Far Field Radiation due to the Surface Currents $\mathbf{J}_s'$, $\mathbf{M}_s'$

The far field due to the equivalent surface current densities $\mathbf{J}_s'$ and $\mathbf{M}_s'$ located at the $z = 0$ plane can be evaluated using (2.11)

$$\mathbf{J}_s' = \hat{\mathbf{z}} \times \mathbf{H_i} = \hat{\mathbf{z}} \times (\hat{\rho} H_\rho + \hat{o} H_o + \hat{\mathbf{z}} H_z) = \hat{o} H_\rho - \hat{\rho} H_o$$
$$\mathbf{M}_s' = -\hat{\mathbf{z}} \times \mathbf{E_i} = -\hat{\mathbf{z}} \times (\hat{\rho} E_\rho + \hat{o} E_\phi + \hat{\mathbf{z}} E_z) = \hat{\rho} E_o - \hat{o} E_\rho \tag{5.5}$$

which in rectangular coordinates become

$$J_{sx} = -\sin o' H_\rho - \cos o' H_\phi$$
$$J_{sy} = \cos o' H_\rho - \sin o' H_\phi$$
$$M_{sx} = \cos o' E_o + \sin o' E_\rho$$
$$M_{sy} = \sin o' E_o - \cos o' E_\rho \tag{5.6}$$

Since $\mathbf{J}_s'$ and $\mathbf{M}_s'$ are two-dimensional surface current densities with no z components. the fields in (5.3) become

$$E_\theta^s = -j\omega\mu(\cos\theta \cos oA_x + \cos\theta \sin oA_y) - jk_0(-\sin oF_x + \cos oF_y)$$
$$E_o^s = -j\omega\mu(-\sin oA_x + \cos oA_y) + jk_0(\cos\theta \cos oF_x + \cos\theta \sin oF_y) \tag{5.7}$$

while the vector potentials $\mathbf{A}$ and $\mathbf{F}$ become

$$\mathbf{A} = \frac{\epsilon^{-jk_0 r}}{4\pi r} \int_0^{2\pi} \int_0^{\infty} [\hat{\mathbf{x}}(-sin\phi' H_\rho - \cos o' H_\phi) + \hat{\mathbf{y}}(\cos o' H_\rho - \sin\phi' H_o)]$$
$$\cdot \epsilon^{jk_0 \rho' \sin\theta \cos(\phi - \phi')} \rho' \, d\rho' \, d\phi'$$
$$\mathbf{F} = \frac{\epsilon^{-jk_0 r}}{4\pi r} \int_0^{2\pi} \int_0^{\infty} [\hat{\mathbf{x}}(\cos\phi' E_\phi + \sin\phi' E_\rho) + \hat{\mathbf{y}}(\sin\varphi' E_\phi - \cos\varphi' E_\rho)]$$
$$\cdot \epsilon^{jk_0 \rho' \sin\theta \cos(\phi - \phi')} \rho' \, d\rho' \, d\phi' \tag{5.8}$$

where the volume integrals have been reduced to surface integrals since the equivalent source consists of the surface currents $\mathbf{J}_s'$ and $\mathbf{M}_s'$ located in the plane $z = 0$.

5.1.1 HE_{11} mode

Evaluation of the expressions for the vector potentials using the fields for the HE_{11} mode as obtained in Chapter 3 yield the following radiation fields due to the equivalent surface currents $\mathbf{J}_s'$ and $\mathbf{M}_s'$ [5].

$$E_\theta^s = \frac{|E_{rad}|\epsilon^{-jk_0r}}{4\pi r}\int_0^{2\pi}\left\{\frac{1}{u}\int_0^a\left\{[-A_1\rho' J_0(u\rho') - A_2J_1(u\rho')]g_1(o')\sin(o-o')\right.\right.$$
$$\left.+[A_3\rho' J_0(u\rho') - A_2J_1(u\rho')]f_1(o')\cos(o-o')\right\}\epsilon^{jk_0\rho'\sin\theta\cos(o-o')}d\rho'$$
$$+\frac{J_1(ua)}{wK_1(wa)}\int_a^\infty\left\{[-A_1\rho' K_0(w\rho') - A_4K_1(w\rho')]g_1(o')\sin(o-o')\right.$$
$$\left.\left.+[A_5\rho' K_0(w\rho') - A_4K_1(w\rho')]f_1(o')\cos(o-o')\right\}\epsilon^{jk_0\rho'\sin\theta\cos(o-o')}d\rho'\right\}do' \quad (5.9)$$

$$E_o^s = \frac{|E_{rad}|\epsilon^{-jk_0r}}{4\pi r}\int_0^{2\pi}\left\{\frac{1}{u}\int_0^a\left\{[-B_1\rho' J_0(u\rho') - B_2J_1(u\rho')]g_1(o')\cos(o-o')\right.\right.$$
$$\left.-[B_3\rho' J_0(u\rho') - B_2J_1(u\rho')]f_1(o')\sin(o-o')\right\}\epsilon^{jk_0\rho'\sin\theta\cos(o-o')}d\rho'$$
$$+\frac{J_1(ua)}{wK_1(wa)}\int_a^\infty\left\{[-B_1\rho' K_0(w\rho') - B_4K_1(w\rho')]g_1(o')\cos(o-o') -\right.$$
$$\left.\left.-[B_5\rho' K_0(w\rho') - B_4K_1(w\rho')]f_1(o')\sin o-o')\right\}\epsilon^{jk_0\rho'\sin\theta\cos(o-o')}d\rho'\right\}do' \quad (5.10)$$

where

$$A_1 = \omega\mu_0\gamma_1(k_0+\beta\cos\theta) \qquad B_1 = \omega\mu_0\gamma_1(\beta+k_0\cos\theta)$$
$$A_2 = \frac{1}{u}(A_3 - A_1) \qquad B_2 = \frac{1}{u}(B_3 - B_1)$$
$$A_3 = k_0\beta + k_1^2\cos\theta \qquad B_3 = k_0\beta\cos\theta + k_1^2$$
$$A_4 = \frac{1}{w}(A_1 - A_5) \qquad B_4 = \frac{1}{w}(B_1 - B_5)$$
$$A_5 = k_0\beta + k_2^2\cos\theta \qquad B_5 = k_0\beta\cos\theta + k_2^2$$

and where $f_1(o')$ and $g_1(o')$ are given by (3.17) and (3.18) respectively, with o replaced by o'.

5.1.2 TE_{01} mode

A similar evaluation of the vector potentials and surface currents for the TE_{01} mode using the field expressions derived in Chapter 3, yields

$$E_\theta^s = \frac{|H_{rad}|\epsilon^{-jk_0r}\omega\mu_0}{4\pi r}\left[\int_0^{2\pi}\sin(\phi-\phi')d\phi\left\{\int_0^a\frac{J_1(u\rho')\rho'}{u}f(\rho',\phi')\right.\right.$$
$$\left.\left.\cdot(\beta\cos\theta+k_0)d\rho' + \int_a^\infty\alpha\frac{K_1(w\rho')\rho'}{w}f(\rho',\phi')(\beta\cos\theta+k_0)d\rho'\right\}\right] \quad (5.11)$$

$$E_\phi^s = \frac{|H_{rod}|\epsilon^{-jk_0 r}\omega\mu_0}{4\pi r}\left[\int_0^{2\pi}\cos(\phi-\phi')d\phi'\left\{\int_0^a \frac{J_1(u\rho')\rho'}{u}f(\rho',\phi')\right.\right.$$
$$\left.\left.\cdot(\beta+k_0\cos\theta)d\rho' + \int_a^\infty \frac{aK_1(w\rho')\rho'}{w}f(\rho',\phi')(beta+k_0\cos\theta)d\rho'\right\}\right] \quad (5.12)$$

5.2 Far Field Radiation due to the Volume Current Density $\mathbf{J_v}$

The far-field due to the equivalent "fictitious" volume current density $\mathbf{J_v}$ within the dielectric cone can be evaluated by (2.14):

$$\mathbf{J_v} = j\omega\epsilon_0(n_1^2-1)\mathbf{E_c} = j\omega\epsilon_0(n_1^2-1)(\hat{\rho}E_{\rho 1}+\hat{\phi}E_{\phi 1}+\hat{\mathbf{z}}E_{z1}) = \hat{\rho}J_\rho+\hat{\phi}J_\phi+\hat{\mathbf{z}}J_z \quad (5.13)$$

which in terms of rectangular components becomes

$$\mathbf{J_v} = j\omega\epsilon_0(n_1^2-1)[(\hat{\mathbf{x}}\cos\phi'+\hat{\mathbf{y}}\sin\phi')E_\rho^c+(-\hat{\mathbf{x}}\sin\phi'+\hat{\mathbf{y}}\cos\phi')E_\phi^c+\hat{\mathbf{z}}E_z^c \quad (5.14)$$

The far field can now be evaluated from (5.3). Since there is no magnetic current distribution $\mathbf{M}$ defined in the conical region, the vector potential $\mathbf{F}=\mathbf{0}$ in this region. Thus, (5.3) reduces to

$$E_\theta^c = -j\omega\mu(\cos\theta\cos\phi A_x+\cos\theta\sin\phi A_y-\sin\theta A_z)$$
$$E_\phi^c = -j\omega\mu(-\sin\phi A_x+\cos\phi A_y) \quad (5.15)$$

where

$$\mathbf{A} = j\omega\epsilon_0(n_1^2-1)\frac{\epsilon^{-jk_0 r}}{4\pi r}\int_0^L\int_0^{2\pi}\int_0^{a(z')}[\hat{\mathbf{x}}(\cos\phi' E_\rho^c-\sin\phi' E_\phi^c)$$
$$+\hat{\mathbf{y}}(\sin\phi' E_\rho^c+\cos\phi' E_\phi^c)+\hat{\mathbf{z}}E_z^c]\epsilon^{jk_0(\rho'\sin\theta\cos(\phi-\phi')+z'\cos\theta)} \quad (5.16)$$

5.2.1 HE_{11} mode

Evaluation of (5.15) using (4.2) yield the expressions for the radiation field due to the volume current density $\mathbf{J_v}$ [5]:

$$E_\theta^c = k_0^2(n_1^2-1)\frac{\epsilon^{-jk_0r}}{4\pi r}\int_0^L\int_0^{2\pi}\int_0^{a(z')} \mid E_{rod}(z') \mid \left\{\frac{j}{u(z')}\left\{[-\beta(z')\right.\right.$$
$$\cdot\rho'(z')J_0(\gamma)+D_1J_1(\gamma)]f_1(o')\cos\theta\cos(o-o')+\mu\omega Z_E\rho'(z')J_0(\gamma)$$
$$\left.\left.+D_1J_1(\gamma)]g_1(o')\cos\theta\sin(o-o')\right\}-\rho'(z')J_1(\gamma)\sin\theta\cos o'\right\}$$
$$\cdot\epsilon^{jk_0\rho'(z')\sin\theta\cos(o-o')}d\rho'(z')\,do'\,\epsilon^{j[k_0z'\cos\theta-\int_0^{z'}\beta(\xi)d\xi}dz' \qquad (5.17)$$

$$E_o^c = k_0^2(n_1^2-1)\frac{\epsilon^{-jk_0r}}{4\pi r}\int_0^L\int_0^{2\pi}\int_0^{a(z')} \mid E_{rod}(z') \mid \frac{j}{u(z')}$$
$$\cdot\left\{\left[\beta(z')\rho'(z')J_0(\gamma)-D_1J_1(\gamma)\right]f_1(o')\sin(o-o')\right.$$
$$\left.+[\mu\omega Z_E\rho'(z')J_0(\gamma)+D_1J_1(\gamma)]\cdot g_1(o')\cos(o-o')\right\}$$
$$\cdot\epsilon^{jk_0\rho'(z')\sin\theta\cos(o-o')}d\rho'(z')\,do'\,\epsilon^{j[k_0z'\cos\theta-\int_0^{z'}\beta(\xi)d\xi}dz' \qquad (5.18)$$

where

$$D_1(z') = \frac{\beta(z')-\omega\mu_0)\gamma_1}{u(z')}$$

and $\gamma = u(z')\rho(z')$ as adopted in Chapter 4.

5.2.2 TE_{01} mode

To obtain the radiation fields due to the volume current density for the TE_{01} mode. (5.15) is evaluated using (4.3) which results in

$$E_\theta^c = \frac{-j\epsilon^{-jk_0r}}{4\pi r}k_0^2(n^2-1)\omega\mu_0\cos\theta\int_0^L\frac{\mid H_{rod}(z')\mid}{u(z')}\epsilon^{j\left[k_0z'\cos\theta-\int_0^{z'}\beta(\xi)d\xi\right]}dz'$$
$$\cdot\int_0^{2\pi}\sin(\phi-\phi')d\phi'\int_0^{a(z')}J_1(\gamma)\rho'\epsilon^{jk_0\rho'\sin\theta\cos(o-phi')}d\rho' \qquad (5.19)$$
$$E_\phi^c = \frac{-j\epsilon^{-jk_0r}}{4\pi r}k_0^2(n^2-1)\omega\mu_0\int_0^L\frac{\mid H_{rod}(z')}{u(z')}\epsilon^{j\left[k_0z'\cos\theta-\int_0^{z'}\beta(\xi)d\xi\right]}dz'$$
$$\cdot\int_0^{2\pi}\cos(\phi-\phi')d\phi'\int_0^{a(z')}\rho'J_1(\gamma)\epsilon^{jk_0\rho'(z')\sin\theta\cos(\phi-\phi')}d\rho'(z') \qquad (5.20)$$

where again, $\gamma = u(z')\rho(z')$.

5.3 Directive Gain

The directive gain is defined as the ratio of the radiation intensity in a certain direction to the average radiation intensity of an isotropic source.

$$G_d(\theta, o) = \frac{U(\theta, o)}{U_{av}}$$

where

$$U_{av} = \frac{P_{rad}}{4\pi} \approx \frac{P_{in}}{4\pi}$$

considering a lossless dielectric. For the far field, the expression becomes

$$U(\theta, o) \approx \frac{1}{2\eta_0}\left[| E_o(\theta, o) |^2 + | E_\theta(\theta, o) |^2 \right]$$

where $\eta_0 = \sqrt{\mu_0/\epsilon_0}$ is the intrinsic impedance in free space. Thus, the directive gain for a lossless tapered dielectric rod becomes

$$G_d(\theta, o) = \frac{2\pi\left[| E_o(\theta, o) |^2 + | E_\theta(\theta, o) |^2 \right]}{\eta_0 P_{in}} \tag{5.21}$$

where $P_{in} = P_{z<0}$ is the power accepted by the dielectric waveguide as calculated in Chapter 4.

CHAPTER 6
NUMERICAL AND EXPERIMENTAL RESULTS

The theoretical predictions of the previous chapters were compared with the far field radiation pattern generated by dielectric cones excited with the fundamental HE_{11} mode. In order to ensure the accuracy of the experiment, it was necessary to test the radiating patterns of the various waveguides used against suitable theoretical models. The experiments were conducted in an anechoic chamber so as to reduce wave reflections off surrounding objects in the room.

The experimental set-up consisted of a signal generator that excited the fields inside a waveguide of rectangular cross-section. This cross-section was gradually converted into a circular cross-section, thereby forming an open-ended circular waveguide. A mode converter was then attached to the circular waveguide. Finally, a cylindrical dielectric rod with tapered ends was inserted into the mode converter. Fig. 6.1 shows the antenna assembly used in the experiment.

6.1 Radiation Pattern of a Circular Guide

A circular waveguide is excited at one end with the TE_{11} mode and its far field radiation pattern is observed. The angular distribution of the emitted radiation

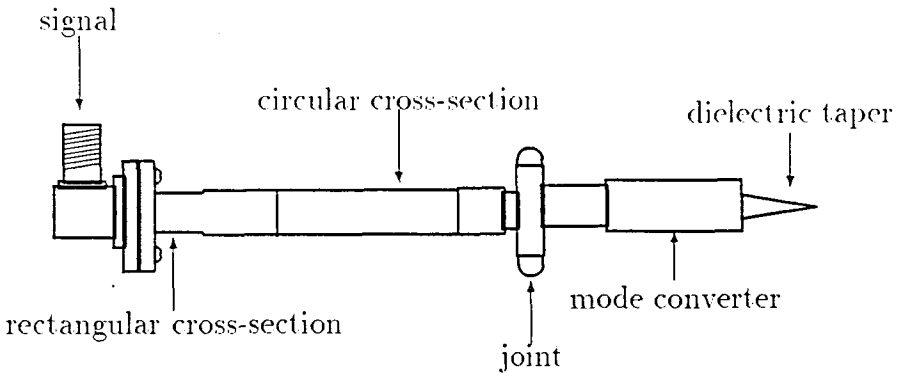

Figure 6.1 Experimental antenna assembly

is compared with the directive gain as predicted by Marcuvitz [8]. The following expression is used to determine the directive gain in the horizontal plane.

$$G(\theta,\phi)=\frac{4k\kappa a^2}{\pi\beta_1'}\frac{J_1(\pi\beta_1')}{H(ka,\kappa a)-H(ka,-\kappa a)}\left[\cos^2\phi\frac{J_1'(ka\sin\theta)}{1-\left(\frac{ka\sin\theta}{\pi\beta_1'}\right)^2}H(ka,ka\cos\theta)\right.$$
$$\left.+2\sin^2\phi\frac{J_1(ka\sin\theta)}{\sin\theta}E(ka,ka\cos\theta)\right] \quad (6.1)$$

where β_1' is defined by $J_1'(\pi\beta_1')=0$ and.

$$H(x,y)=\frac{(x+y)^{5/2}\epsilon^y}{|x+\xi_0 a|^2|y+\xi_0 a|^2}\left|\frac{x-y}{x+y}+jA_2\right|^2$$
$$\cdot\epsilon^{\frac{1}{\pi}\int_0^\infty\frac{tdt}{\sqrt{t^2+x^2}}\left(\frac{1}{\sqrt{t^2+x^2+y}}+\frac{1}{\sqrt{t^2+x^2}+x}\right)\arctan\frac{-K_1'(t)}{\pi I_1'(t)}}$$

$$E(x,y)=\frac{\epsilon^y}{\sqrt{x+y}}\epsilon^{\frac{-1}{\pi}\int_0^\infty\frac{tdt}{\sqrt{t^2+x^2}}\left(\frac{1}{\sqrt{t^2+x^2+y}}+\frac{1}{\sqrt{t^2+x^2}+x}\right)\arctan\frac{K_1(t)}{\pi I_1(t)}} \quad (6.2)$$

The angular distribution as obtained by the above expressions at $\phi=\frac{\pi}{2}$ is plotted along with the observed far field patterns in Fig.6.2. Similar matching patterns were observed over a wide range of frequencies. confirming the excitation of the TE_{11} mode in the circular waveguide. The radiation pattern from hollow pipes has been studied and documented extensively by Chu [9].

6.2 HE_{11} Mode Radiation Pattern

A mode converter is attached to the section of waveguide described above. The TE_{11} field in the circular waveguide is thus converted to a propagating HE_{11} mode. The mode converter used in this experiment was designed by Pietrangelo [10] for a frequency of 15 GHz. Again. the radiation pattern emitted by the open-ended mode converter was compared against the theoretical radiation pattern for the HE_{11} mode as predicted by Thomas [11]. The far field components of the radiating hybrid HE_{11} mode have the following form:

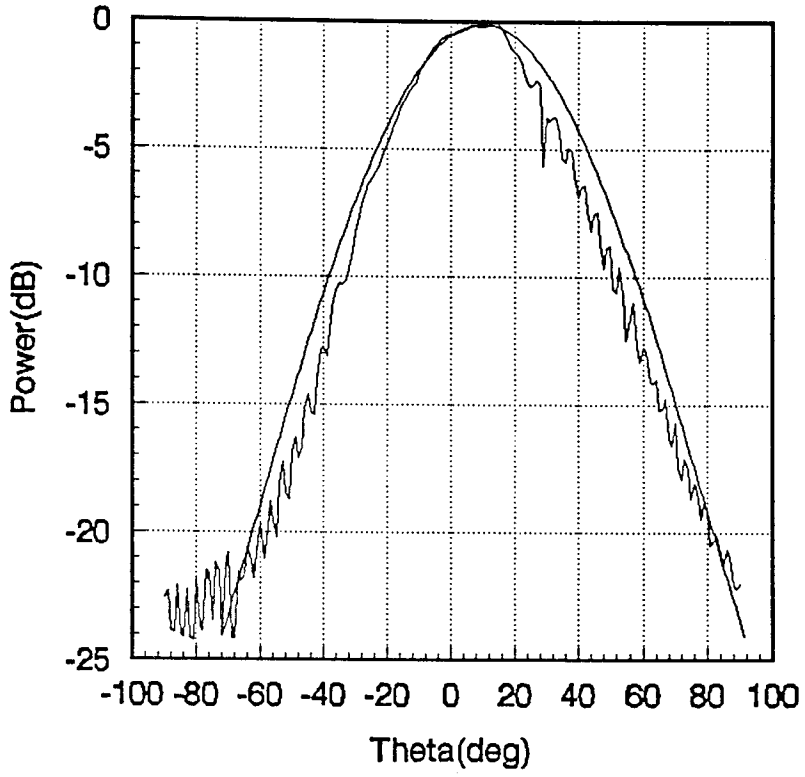

Figure 6.2 TE_{11} mode far field radiation pattern from a semi-infinite circular waveguide with aperture radius=7.5mm at 15GHz.

$$E_v(v) = ka\left[\gamma\left(1+\frac{k_z}{k}\cos\psi\right)K_1 + \left(\frac{k_z}{k}+\cos\psi\right)K_2\right]$$
$$E_\phi(v) = ka\left[\left(1+\frac{k_z}{k}\cos\psi\right)K_1 + \gamma\left(\frac{k_z}{k}+\cos\psi\right)K_2\right] \qquad (6.3)$$

where

$$K_1 = mJ_m(u_a)\frac{J_m(v)}{v}, \quad K_2 = \frac{J_m(u_a)J'_m(v) - \frac{v}{u_a}J_m(v)J'_m(u_a)}{1-\left(\frac{v}{u_a}\right)^2}$$

and the generalized radiation angle $v = ka\sin\psi$. For the axially symmetric HE_{11} mode, $m = 1$ and $v = 0$ along the axial direction. The theoretical results are plotted along with the experimentally observed radiation patterns in Fig 6.3. There is a

good agreement between the two sets of data indicating a satisfactory conversion of the TE_{11} mode into the HE_{11} mode .

The analysis and the design of mode converters using corrugated waveguides has been discussed by various authors. In particular, the reader is referred to articles by Clarricoats[12]. James[13]. Doane[14] and Narasimhan[15].

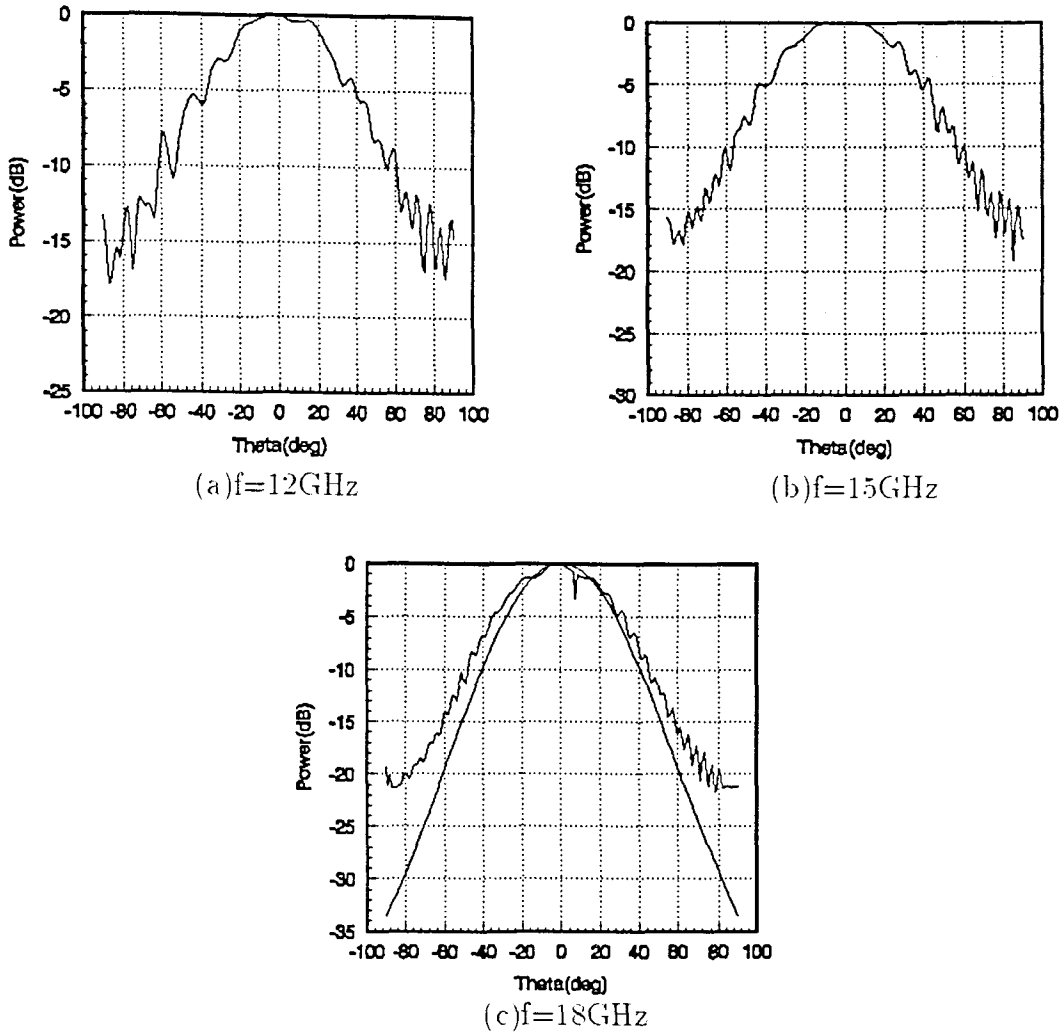

Figure 6.3 HE_{11} mode far field radiation pattern from an open-ended mode converter with guide radius=7.5mm

6.3 Radiation from the Tapered Dielectric

The far field radiation patterns from a tapered dielectric cone excited by the HE_{11} mode were determined previously by Hoydal [5]. An attempt has been made to support his theoretical model with experimental data. For this purpose, a set of three taper lengths was used with two different materials, teflon ($n = 1.449$) and plexiglass ($n = 1.6$). The taper lengths under study were 2.8cm, 1.9cm and 1.5cm long. Figs. 6.5 to 6.10 show the far field radiation patterns for each of the dielectric cones at various frequencies. These patterns are plotted along with the theoretical angular distribution predicted by the discussion in earlier chapters. The surrounding medium in each case is air ($n = 1.0$). Readings were taken for 3 frequencies, 12GHz, 15GHz and 18GHz.

The observations were made in an anechoic chamber using steps of one degree on a rotating stage *UR100PP, Klinger*, controlled by a GPIB board and accompanying software. The controlling program was capable of setting the frequency and power output of the *HP8350B Sweep Oscillator*, controlling the *Motion Master 2000* motor and triggering system and the *Boonton 4200 RF Microwattmeter* to take a reading. The data was then collected and normalized with respect to the 0dBm level and plotted along with the corresponding theoretical radiation pattern.

As can be seen from the plots, longer tapers favor the formation of a main lobe along the axis of the dielectric. However, it was not possible to obtain tapered lengths greater than 2.8cm due to machining difficulties. In order to work with relatively longer tapers, higher frequencies of operation were attempted. Beyond 18GHz, it was no longer feasible to take accurate readings since the base noise level in the anechoic chamber began to interfere with the radiations from the dielectric cone. It was found that 12GHz and 18GHz were the extreme limits of operating frequency possible in this experimental set-up. Readings were taken at each of these 3 frequencies. The higher refractive index of plexiglass allowed better guiding within the dielectric cone

and thus generated more well-defined central lobes. Very good agreement is found between the theoretical and observed data for the plexiglass taper of length 2.8cm. Since the experiments were conducted in a poorly furnished anechoic chamber, the reflections off the walls of the chamber caused distortions in the envelope of the radiation pattern.

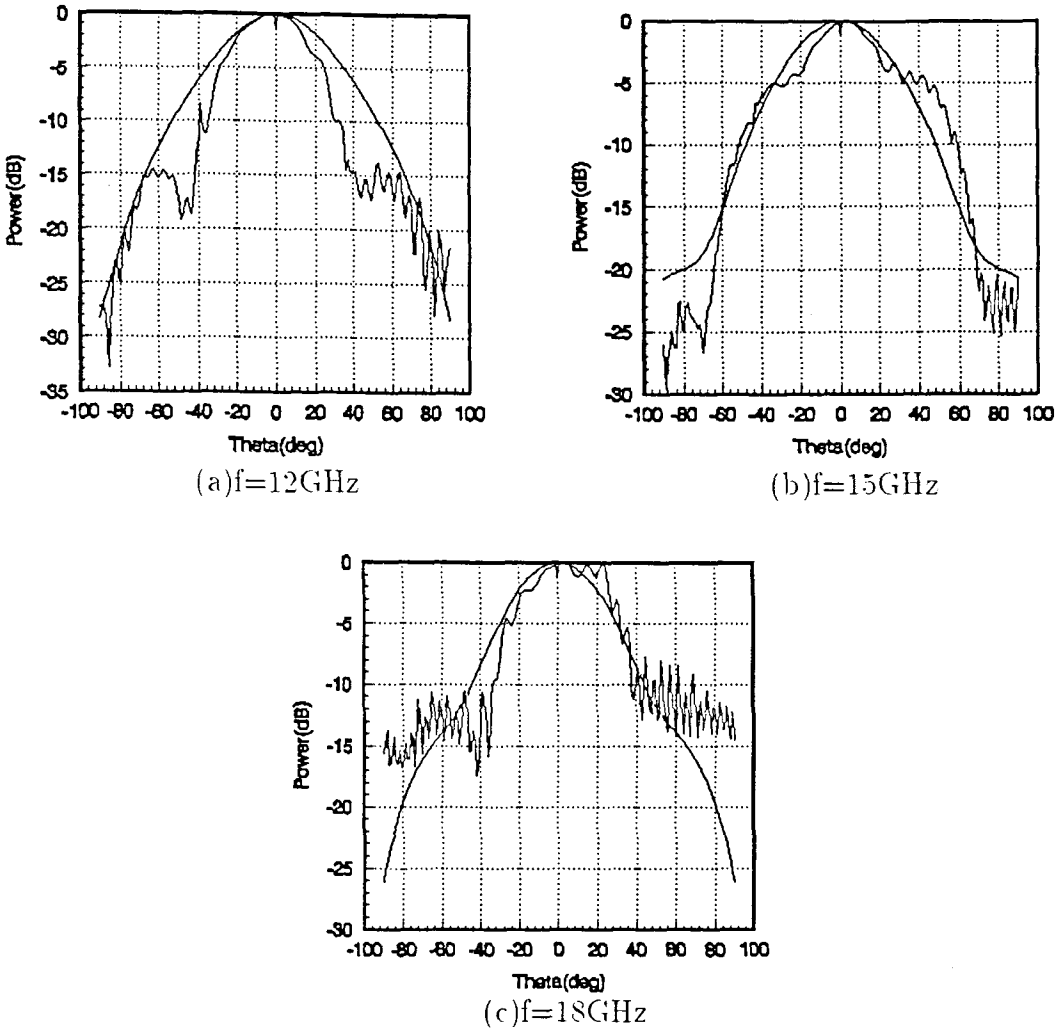

Figure 6.4 HE_{11} mode far field radiation pattern for plexiglass $L = 2.8$cm. $n = 1.6$. $a = 7.5$mm. $r = 1$m. $\phi = 0^{\circ}$

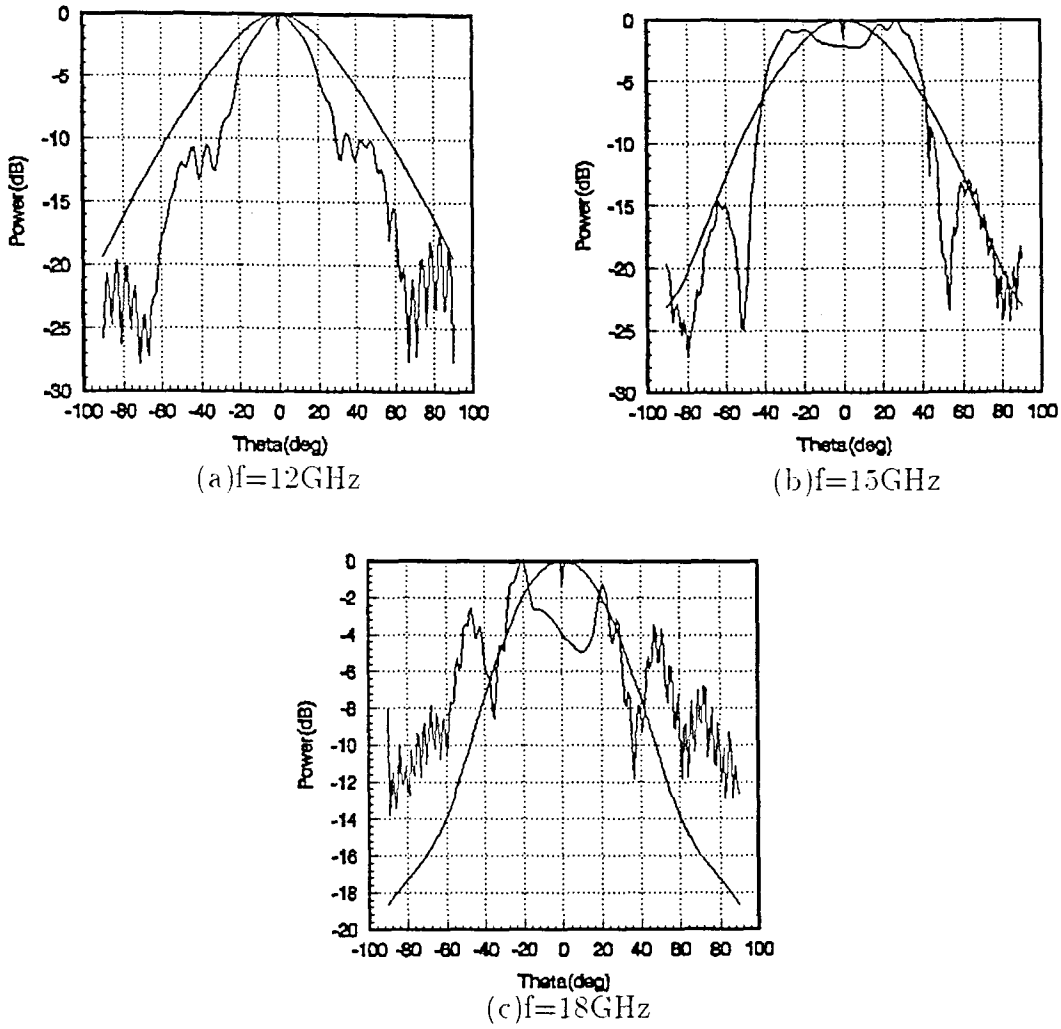

Figure 6.5 HE_{11} mode far field radiation pattern for plexiglass $L = 1.9$cm $n = 1.6$, $a = 7.5$mm, $r = 1$m, $\phi = 0^{\circ}$

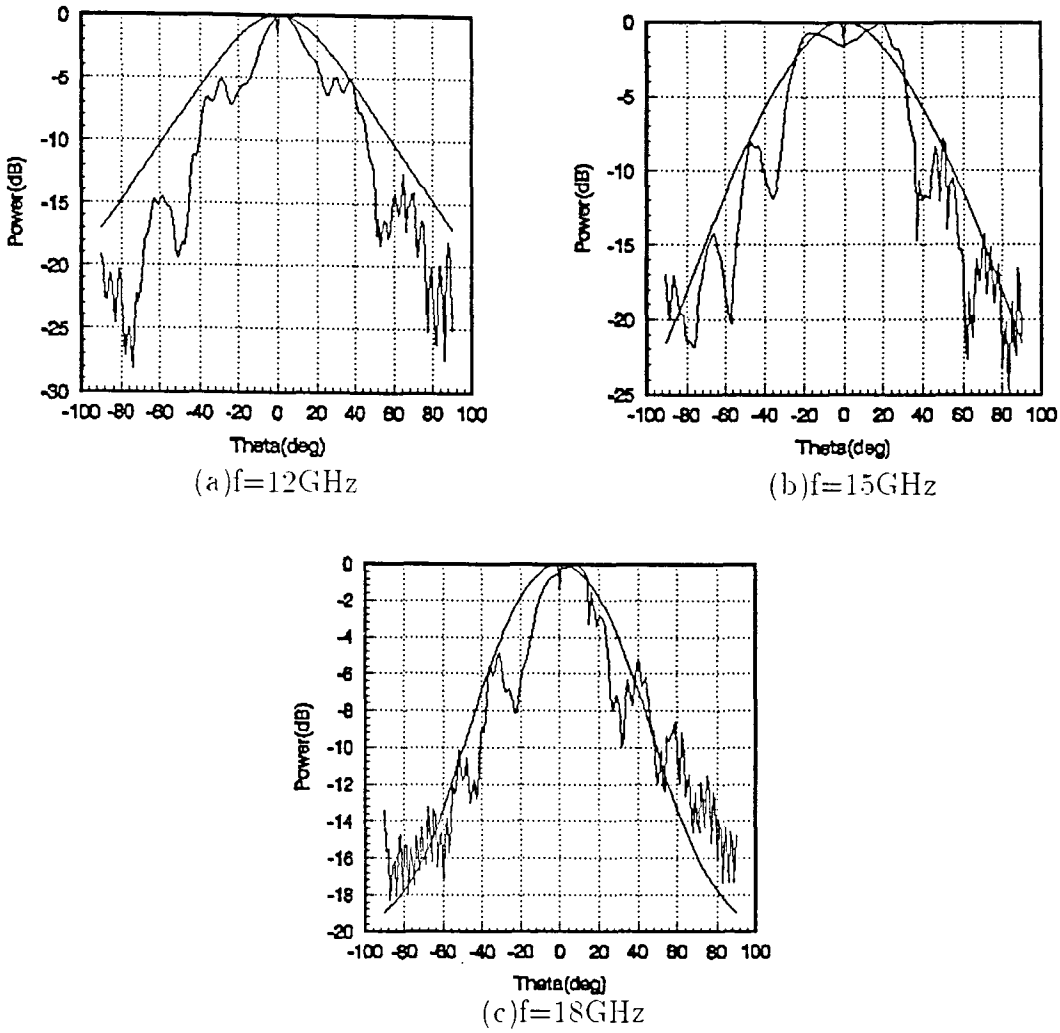

Figure 6.6 HE_{11} mode far field radiation pattern for plexiglass $L = 1.5$cm, $n = 1.6$, $a = 7.5$mm, $r = 1$m, $\phi = 0^{\circ}$

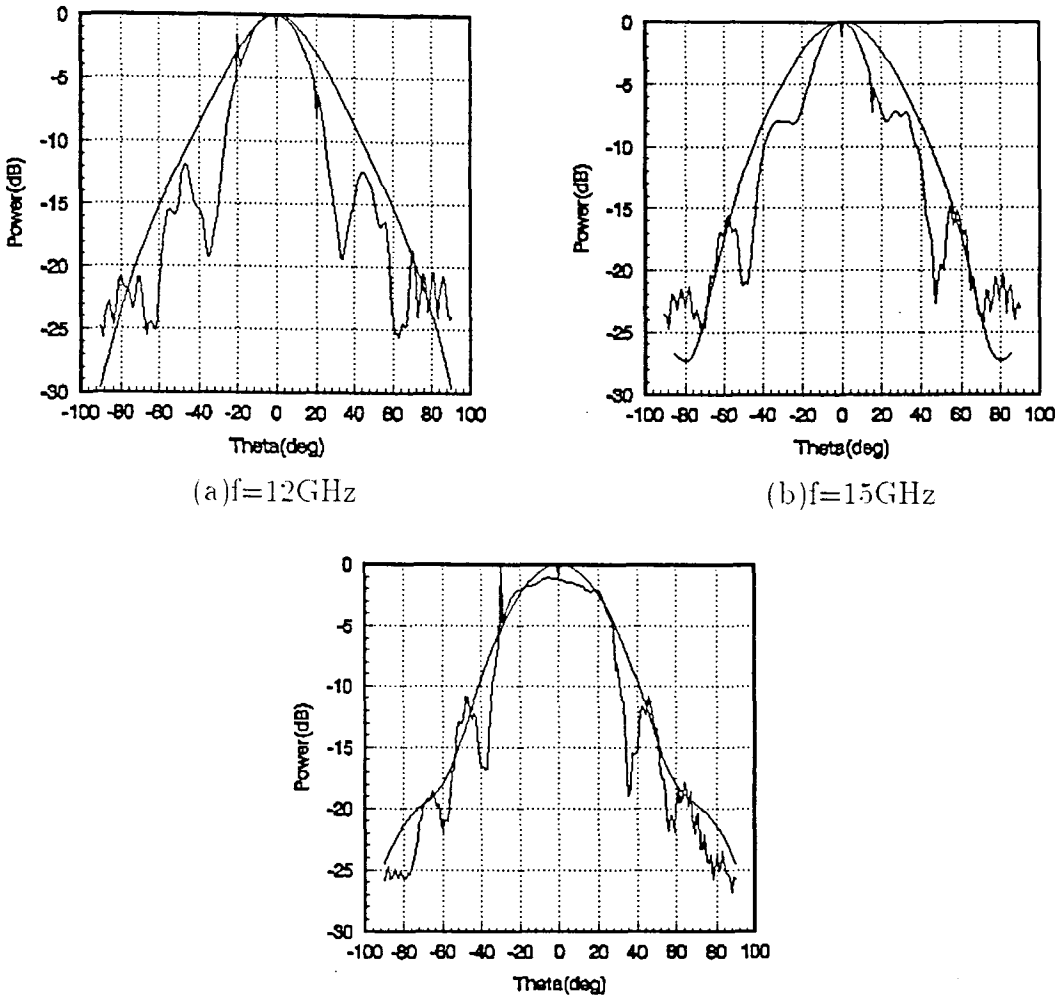

(a)f=12GHz (b)f=15GHz

(c)f=18GHz

Figure 6.7 HE_{11} mode far field radiation pattern for teflon $L = 2.8$cm, $n = 1.449$, $a = 7.5$mm, $r = 1$m, $o = 0^o$

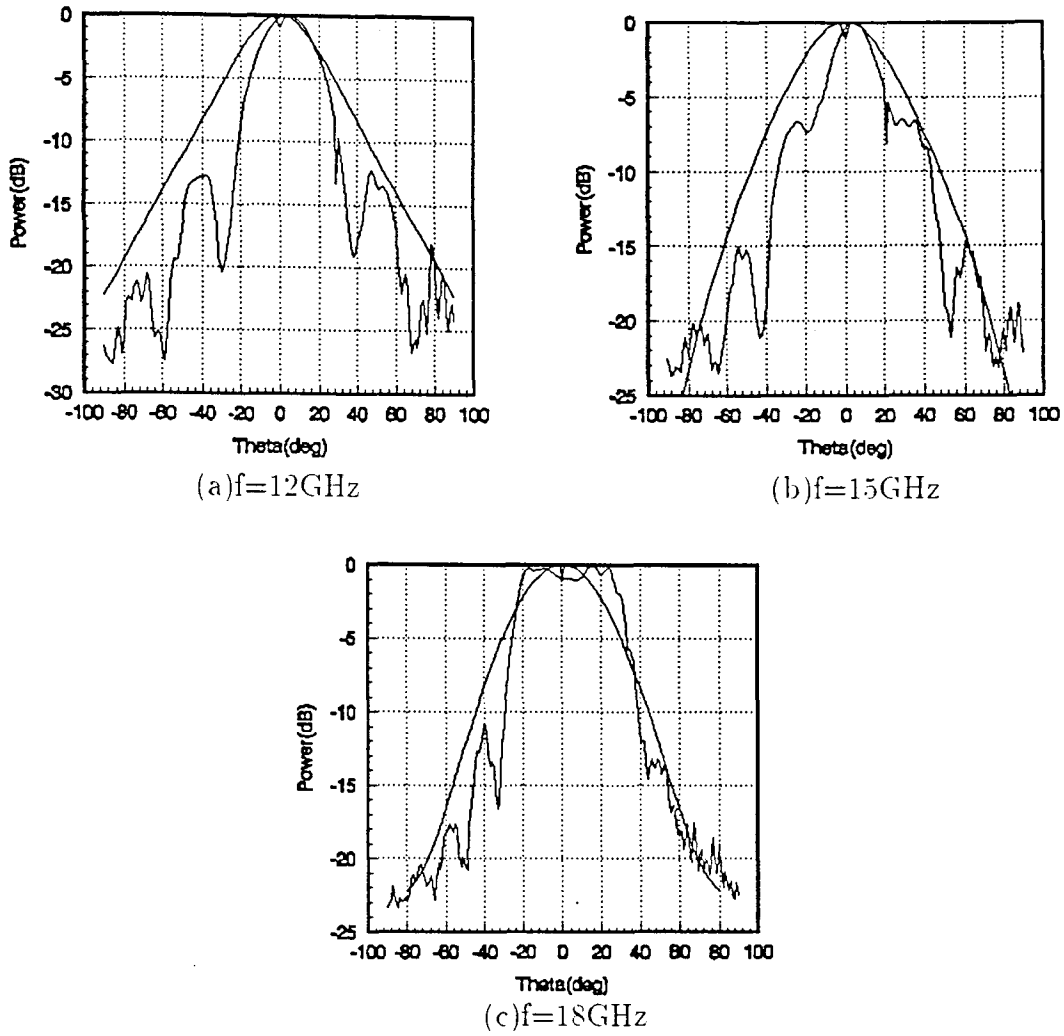

Figure 6.8 HE_{11} mode far field radiation pattern for teflon $L = 1.9$cm. $n = 1.449$. $a = 7.5$mm. $r = 1$m. $\phi = 0^{\circ}$

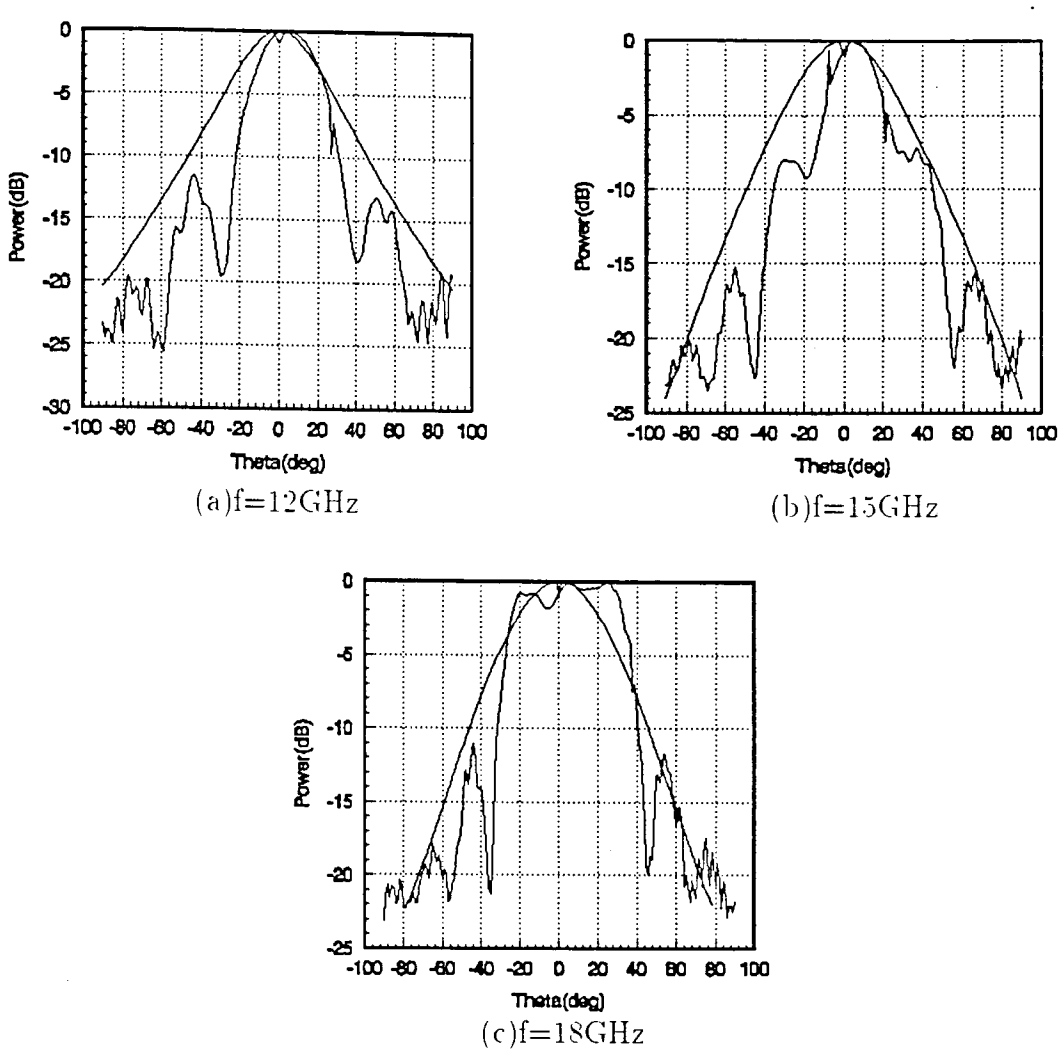

(a)f=12GHz

(b)f=15GHz

(c)f=18GHz

Figure 6.9 HE_{11} mode far field radiation pattern for teflon $L = 1.5$cm. $n = 1.449$. $a = 7.5$mm. $r = 1$m. $\phi = 0^{\circ}$

6.4 TE_{01} Mode Radiation Pattern

Using the theoretical model presented in earlier chapters, the radiation pattern for the TE_{01} mode is obtained. A computer program written in *FORTRAN* uses the Regula Falsi method [17] to compute the root of the eigenvalue equation (3.64). The integrals used in (5.10), (5.12), (5.18) and (5.20) were evaluated using the Romberg Quadrature technique [18]. Although some of the expressions involve complex numbers, the program was implemented so as to reduce the number of operations in the complex domain. This reduced the run time involved in generating the data for the following plots.

It was necessary to use approximate expressions for the root of the eigenvalue equation when very close to and when very far from cut-off. The cut-off for the TE_{01} mode is at $V = 2.405$. The approximation used far from cut-off is [22],

$$U(V) = U(\infty)e^{-\frac{1}{V}}$$

where $U(\infty) = 3.832$ is the second root of the Bessel function.

and close to cut-off is [22]

$$s = \sqrt{U_c^2 - 1}$$

$$U(V) = U_c exp\left(sin^{-1}\frac{s}{U_c} - sin^{-1}\frac{s}{V}\right)$$

where $U_c = 2.405$ is the cut-off value for the normalized frequency.

Keeping in mind the principles that governed the experiments of the previous section, the radiation pattern for the TE_{01} mode have been plotted for the two frequencies, 15GHz and 18GHz. (It has not been possible to work at 12GHz because the frequency does not fall in the regime of a propagating mode. For the TE_{01} mode to propagate, the normalized frequency parameter V must be greater than 2.405.) The refractive indices used are for teflon ($n = 1.45$) and plexiglass ($n = 1.6$) while the surrounding medium is air ($n = 1.0$). Since we have to ensure that $V > 2.405$ throughout the length of the cone, we are forced to stop our integration at a length

delta away from the tip of the cone. This reduces the accuracy of our calculations considerably since the integrals are evaluated till as little as 30% of the actual length of the taper. This being the next propagating mode in the dielectric. after the fundamental HE_{11} mode. one observes that a lot of power is radiated out at an angle to the axis of the dielectric in the form of lobes. Once again. the formation of lobes is favored by longer tapers and higher refractive indices.

Further work is necessary to keep track of the TE_{01} mode as it undergoes cut-off and the evanescent nature of the field has to be built into the model for the remainder of the taper. Experimental verification also has its difficulties. since the source coupling has to be changed to accommodate this particular mode.

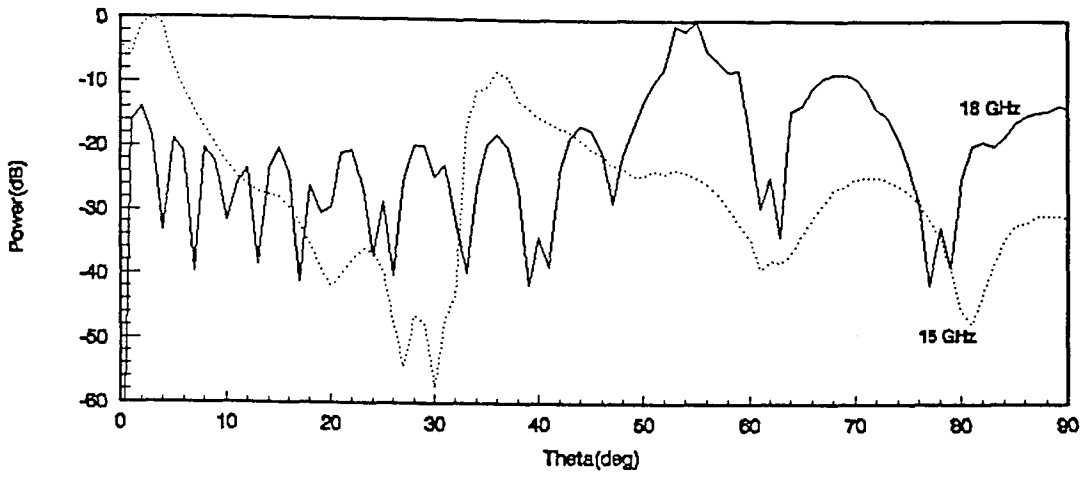

(a)$n = 1.6$

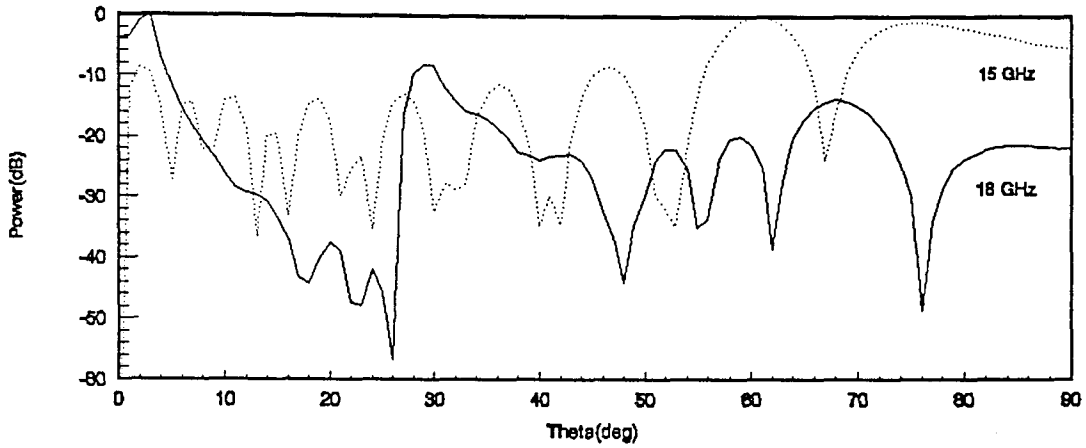

(b)$n = 1.45$

Figure 6.10 TE_{01} mode far field radiation pattern $L = 2.8$cm. $a = 7.5$mm. $r = 1$m. $o = 0^{\circ}$

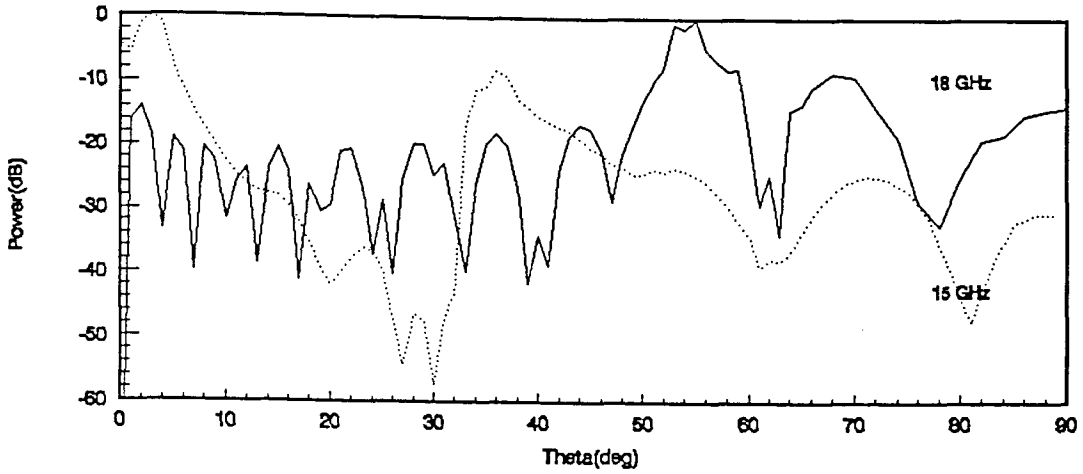

(a)$n = 1.6$

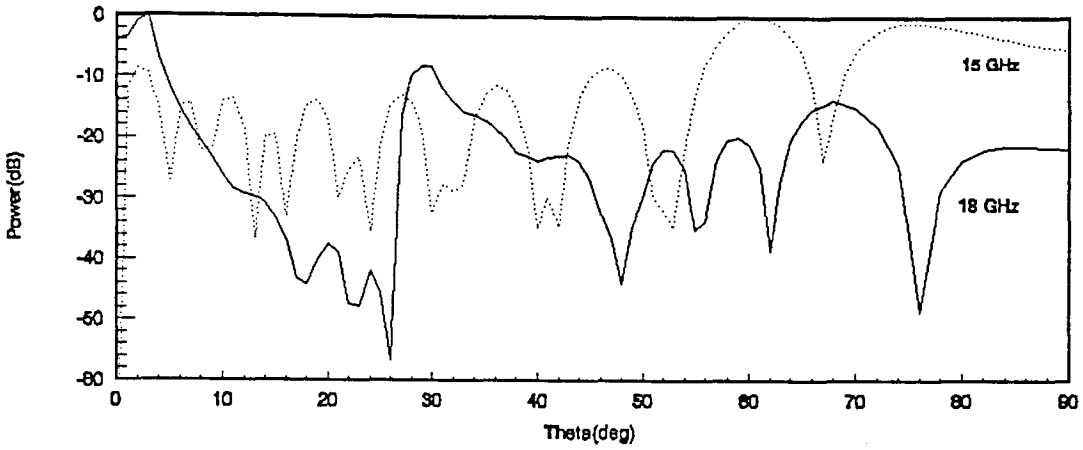

(b)$n = 1.45$

Figure 6.11 TE_{01} mode far field radiation pattern $L = 1.9$cm. $a = 7.5$mm. $r = 1$m. $o = 0^{\circ}$

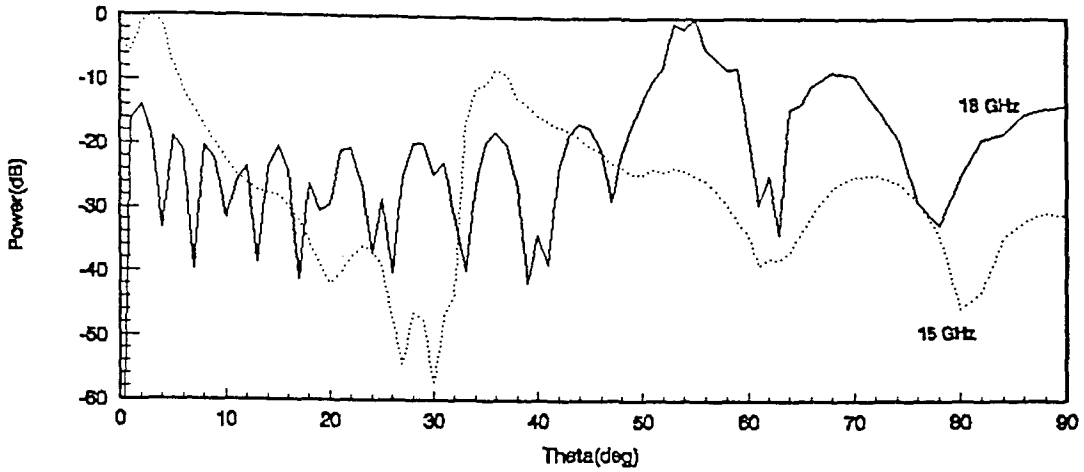

(a)$n = 1.6$

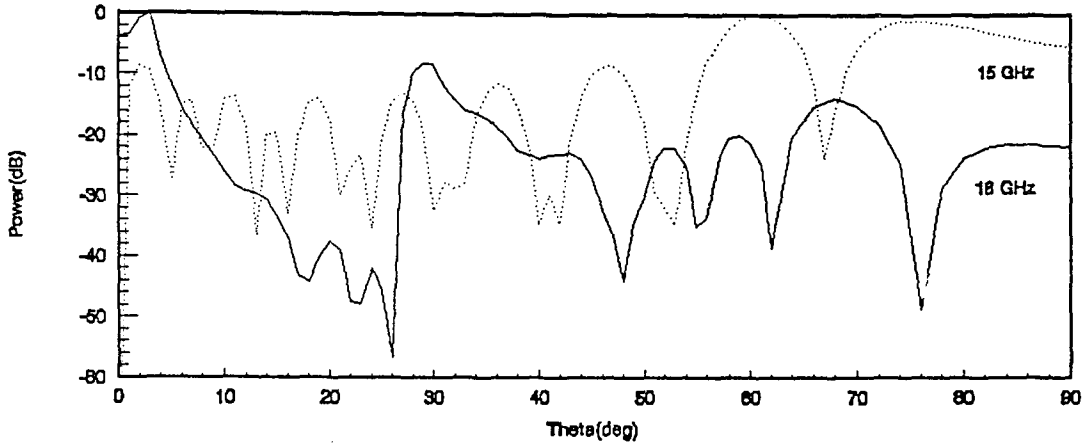

(b)$n = 1.45$

Figure 6.12 TE_{01} mode far field radiation pattern $L = 1.5$cm, $a = 7.5$mm, $r = 1$m, $o = 0^{\circ}$

CHAPTER 7
CONCLUSIONS

The use of the *local mode theory* and the principles of *power conservation* to model the linear tapering of a cylindrical dielectric rod has produced satisfactory results when theory is compared with experimental measurements. However, the results have been studied purely in the microwave frequency range. The major reason for being unable to extend our study to optical wavelengths was the inability of the computer program to generated numerically accurate data when working with extremely short wavelengths as encountered in the optical region. The highly oscillatory nature of the integrals combined with the high degree of accuracy required (double precision proved insufficient to check underflow errors) proved to be a hurdle that is still to be overcome. It has been suggested that in order to evaluate the surface current and volume current density integrals, one should take advantage of the oscillatory nature and attempt to apply *stationary phase* solutions.

Another aspect that has been sidelined is the possibility of multiple reflections off the surface of each concentric cylinder, the combination of concentric cylinders forming the adiabatic approximation to the taper. It appears that such reflections are relatively small for frequencies in the microwave region. When one begins to operate in the optical domain, the extremely short wavelengths, as compared to the dimensions of the taper, may make these reflections significant and may have to be given due consideration by incorporating more accurate models based on the proper treatment of discontinuities [23].

The program for the HE_{11} mode takes about 2 seconds of CPU-time for each reading while executing on a DEC system 5900 (RISC processor). This run-time is considerably reduced for the TE_{01} mode, which takes about 1 second of CPU-time for each reading. This saving in execution time is largely due to the cylindrical symmetry of the TE_{01} that results in much simpler expressions for the eigenvalue equations and

the integrals. Since the data was being generated for the microwave frequencies. the execution times involved were bearable. It is suggested that the programs be modified to take advantage of the optimization capabilities of the compiler before being run in the optical regime. The run-times involved for optical wavelengths are as high as 4 seconds of CPU-time for each reading. Profiling information for the programs reveals that most of the execution time (up to 70%) is spent in the evaluation of *Bessel* and *Modified Bessel* functions. It may be worthwhile to rewrite these subroutines in a more efficient manner. As mentioned in Chapter 6. efforts were made to rewrite the programs using real numbers. Since each operation in the complex domain actually averages to about 5 operations with real numbers. the use of complex numbers in time-consuming routines should definitely be avoided.

From the experimental aspect. the inaccuracies in the readings that arise from the reflections off the walls of the anechoic chamber can be avoided by using a larger chamber with more efficient absorbers. Due to the intrinsic noise level at -50dBm. readings could not be taken at frequencies higher than 18 GHz since the power readings began to fall below the noise level. It is expected that at higher frequencies. the observed angular distribution of power closely matches the theoretical prediction because of the increasing accuracy of the adiabatic approximations made. Judging from the nature of the graphs obtained at the current frequencies. one can hope to attain near perfect correlation between the observed and predicted angular radiation patterns.

REFERENCES

1. A. A. Kishk, L. Shafai, " Radiation Characteristics of the Short Dielectric Rod Antenna: A Numerical Solution," *IEEE Transactions on Antennas and Propagation*, vol. AP-35, No. 2, Feb. 1987.

2. A. W. Snyder and J. D. Love, *Optical Waveguide Theory*, Chapman and Hall Ltd., London, 1983.

3. A. D. Yaghjian and Kornhauser, " A Modal Analysis of the Dielectric-rod Antenna Excited by the HE_{11} Mode," *IEEE Transactions on Antennas and Propagation*, vol. AP-20, pp. 122-128, 1972.

4. N. I. Georghiades, "The Tapered Dielectric Rod-Conical Antenna," Master Thesis, *New Jersey Institute of Technology*, 1988.

5. Tor-Odd Hoydal, "Radiation from the Cylindrical Dielectric Taper," Masters Thesis, *New Jersey Institute of Technology*, 1991.

6. M. Abramowitz and I. A. Stegun, *Handbook of Mathematical Functions*, Dover, New York, 1972.

7. R. F. Harrington, *Time Harmonic Electromagnetic Fields*, McGraw-Hill, New York, 1961.

8. N. Marcuvitz, *Wareguide Handbook*, McGraw-Hill, New York, 1951.

9. L. J. Chu, "Calculation of the Radiation Properties of Hollow Pipes and Horns'," *Journal of Applied Physics*, vol. 11, pp. 603-610, 1940.

10. G. Pietrangelo, "Design of a TE_{11} to HE_{11} Mode Convertor'," Senior Project, *New Jersey Institute of Technology*, 1989.

11. B. MacA. Thomas, "Theoretical Performance of Prime- Focus Paraboloids using Cylindrical Hybrid-Mode Feeds," *Proc. IEEE* , vol.118, pp. 1539-1549, Nov 1971.

12. P. J. B. Clarricoats, "Propagation and Radiation Behaviour of Corrugated Feed," *Proc. IEE*, vol. 118, No. 9, pp. 1167-1176, 1971.

13. G. L. James, "Analysis and Design of TE_{11} to HE_{11} Corrugated Cylindrical Waveguide Mode Convertors," *IEEE Trans. on Microwave Theory and Techniques*, vol. MTT-29, No. 10, pp. 1059-1065, 1981.

14. J. L. Doane, "Mode Convertors for Generating the HE_{11} (Gaussian-like) Mode from TE_{01} in a Circular Waveguide", *Int. J. Electronics*, vol. 53, No. 6, pp. 573-585, 1982.

15. M. S. Narasimhan and K. R. Govind. "Radiation Characteristics of a Corrugated Circular Cylindrical Waveguide Horn Excited in the TE_{11} mode." *IEEE Trans. on Antennas and Propagation*, vol 36, No. 8, pp. 1147-1152, 1988.

16. J. R. James. "Engineering Approach to the Design of Tapered Dielectric-rod and Horn Antennas." *The Radio and Electronic Engineer*, vol. 42, No. 6, 1972.

17. W.H. Press, B. P. Flannery, S. A. Teukolsky, W. T. Vetterling. *Numerical Recipes, The Art of Scientific Computing*, 1989.

18. E. K. Miller. "A Variable Interval Width Quadrature Technique Based on Romberg's Method." *J. Comp. Physics*, vol.5, pp. 265-279, 1970.

19. P. K. Tien, G. Smolinsky, and R. J. Martin. "Radiation Fields of a Tapered Film and a Novel Film-to-Fiber Coupler." *IEEE Trans. on Microware Theory and Techniques*, MTT-23, no. 1, pp. 79-85, Jan. 1975.

20. C. T. Chang and D. C. Auth. "Radiation Characteristics of Tapered Cylindrical Optical Fiber." *J. Opt. Soc. Am.*, vol. 68, no. 9, pp. 1191-1196, Sept. 1978.

21. P. J. Shah. "Tapered Fiber HE_{11} Mode Radiation Pattern Analysis." Senior Project. *New Jersey Institute of Technology*, 1989.

22. A. W. Snyder. "Asymptotic Expressions for Eigenfunctions and Eigenvalues of a Dielectric or Optical Waveguide." *IEEE Trans. on Microware Theory and Techniques*, vol. MTT-17, No. 12, pp. 1130-1138, 1969.

23. T. E. Rozzi. "Rigorous Analysis of the Step Discontinuity in a Planar Dielectric Waveguide." *IEEE Trans. on Microware Theory and Techniques*, vol. MTT-26, No. 10, pp. 738-746, 1978.